This is a repository copy of *An NF-κB Transcription-Factor-Dependent Lineage-Specific Transcriptional Program Promotes Regulatory T Cell Identity and Function*.

Version: Accepted Version

An NF-κB transcription factor-dependent, lineage specific transcriptional program promotes regulatory T cell identity and function

Hyunju Oh[1,9], **Yenkel Grinberg-Bleyer**[1,9], **Will Liao**[2], **Dillon Maloney**[2], **Pingzhang Wang**[3], **Zikai Wu**[3], **Jiguang Wang**[3], **Dev M. Bhatt**[1], **Nicole Heise**[4], **Roland M. Schmid**[5], **Matthew S. Hayden**[1,6], **Ulf Klein**[1,4,7,8], **Raul Rabadan**[3], and **Sankar Ghosh**[1,*]

[1]Department of Microbiology & Immunology, Columbia University College of Physicians & Surgeons, New York, NY 10032

[2]New York Genome Center, New York, NY 10013

[3]Department of Systems Biology and Department of Biomedical Informatics, Columbia University College of Physicians and Surgeons, New York, NY 10032

[4]Herbert Irving Comprehensive Cancer Center, College of Physicians & Surgeons, Columbia University, New York, NY 10032, USA

[5]II Medizinische Klinik, Klinikum Rechts der Isar, Technische Universität Munich, Munich, Germany

[6]Section of Dermatology, Department of Surgery, Dartmouth-Hitchcock Medical Center, Lebanon, New Hampshire, 03756, USA

[7]Department of Pathology & Cell Biology, College of Physicians & Surgeons, Columbia University, New York, NY 10032, USA

Summary

Both conventional T (Tconv) cells and regulatory T (Treg) cells are activated through ligation of the T cell receptor (TCR) complex, leading to the induction of the transcription factor NF-κB. In Tconv cells, NF-κB regulates expression of genes essential for T cell activation, proliferation and function. However the role of NF-κB in Treg function remains unclear. We conditionally deleted canonical NF-κB members p65 and c-Rel in developing and mature Treg cells and found they

*Lead contact. Columbia University, Department of Microbiology and Immunology, 701W 168th Street, HHSC 1204, New York, NY 10032, USA. sg2715@cumc.columbia.edu; Tel: (1) 212-342-5424; Fax: (1) 212-305-1468.
[8]Current affiliation: Section of Experimental Haematology, Leeds Institute of Cancer and Pathology, University of Leeds, Leeds LS2 9JT, U.K.
[9]These authors contributed equally

have unique but partially redundant roles. c-Rel was critical for thymic Treg development while p65 was essential for mature Treg identity and maintenance of immune tolerance. Transcriptome and NF-κB p65 binding analyses demonstrated a lineage specific, NF-κB-dependent transcriptional program, enabled by enhanced chromatin accessibility. These dual roles of canonical NF-κB in Tconv and Treg cells highlight the functional plasticity of the NF-κB signaling pathway and underscores the need for more selective strategies to therapeutically target NF-κB.

Graphical abstract
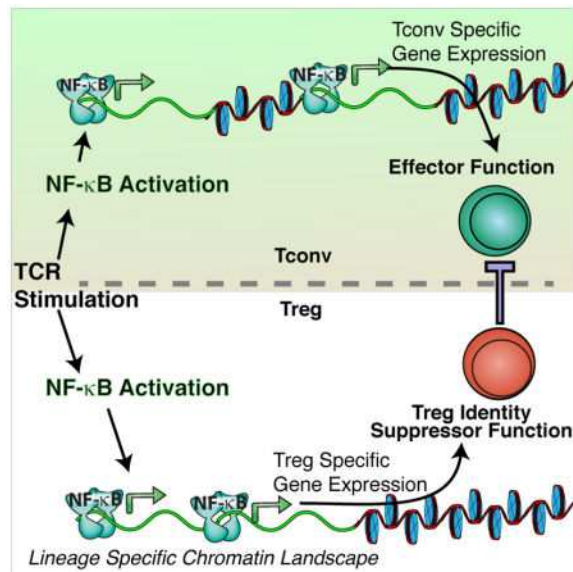
INTRODUCTION

Homeostasis of the immune system is maintained by a delicate balance between activation and suppression. Disruption of this balance can lead to autoimmune diseases and immune dysfunction. Immune tolerance is maintained through central and peripheral mechanisms, including specialized cell subsets. Amongst these, CD4$^+$FoxP3$^+$ regulatory T cells (Treg cells) play a pivotal role in the inhibition of immune responses. Treg cells, which develop in the thymus or in the periphery, are characterized by the expression of the transcription factor FoxP3, and by their ability to suppress the activation and function of conventional T cells (Tconv), and other immune cells, to maintain immune homeostasis. Thus, although they arise from the same progenitors in the thymus, Tconv and Treg cells have completely opposed biological roles. Remarkably, it is still unclear how engagement of the same T cell receptor on these two related cell types induces such different biological outcomes, despite the fact that many of the same signaling molecules and transcription factors are activated (Levine et al., 2014).

The NF-κB transcription factor family consists of five members, p65 (RelA), c-Rel (encoded by *Rela* and *Rel*, respectively), p105/p50, p100/p52 and RelB. NF-κB is activated in response to a variety of signals through two distinct pathways that are known as the

canonical and noncanonical pathways. The canonical pathway leads to activation of NF-κB heterodimers containing primarily p65 or c-Rel, bound to p50, whereas the noncanonical pathway leads to activation of NF-κB heterodimers consisting of RelB and p52. Stimulation of the TCR together with costimulation of CD28 leads to activation of canonical NF-κB complexes, which translocate to the nucleus, where they bind to specific sites in promoters and enhancers of target genes. Thus, in Tconv cells, NF-κB induces expression of genes responsible for T cell activation, proliferation and production of inflammatory cytokines. Given the well-documented role for NF-κB in activation of a variety of immune effector cells, it was unclear what role NF-κB might play in Treg cells, whose biological function is to suppress the immune response.

We, along with other groups, have shown previously that NF-κB c-Rel plays an essential role in the thymic development of Treg cells (Isomura et al., 2009; Long et al., 2009; Ruan et al., 2009). In Treg precursors, c-Rel binds directly to the CNS3 enhancer region and promotes the expression of FoxP3. Treg development is impaired in mice lacking c-Rel and hence the role of NF-κB in Treg function has remained unexplored. To determine how NF-κB contributes to mature Treg function we have now conditionally deleted floxed alleles of NF-κB *Rela* and *Rel* in Tregs. We found that both c-Rel and p65 played important, but only partly redundant roles in Treg function, and only deletion of both c-Rel and p65 led to completely non-functional Tregs and lethal autoimmunity, similar to that seen in mice lacking Tregs. Analysis of the gene expression program in these cells revealed that expression of several key genes that are known to be critical for Treg identity and function was NF-κB-dependent. This suggested that NF-κB was able to access different target genes in Treg and Tconv cells. Genome-wide p65 ChIPseq revealed a large number of lineage specific target genes in Treg cells, associated with an enhanced open chromatin conformation in Tregs. Therefore, our results suggested that an altered global chromatin state in Tregs allows NF-κB induced by the TCR to access lineage-specific binding sites and establish Treg identity and suppressive function. In summary, the studies presented here reveal the plasticity of a key transcription factor in regulating the diametrically opposed biological functions of two highly related cell types.

RESULTS

Canonical NF-κB signaling is crucial for Treg development

We explored the specific roles of the canonical NF-κB subunits c-Rel and p65 in natural (n)Treg and induced (i)Treg development by crossing mice with floxed *Rel* and *Rela* alleles with a *Cd4*[cre] deleter strain resulting in loss of p65 and c-Rel expression (Figure S1A). We did not observe changes in development of CD4^{+} and CD8^{+} T cells in the thymus (data not shown). However, we observed a dramatic decrease in the proportion and number of CD4^{+}CD8^{−}FoxP3^{−}CD25^{+}GITR^{+} Treg precursors in mice lacking p65 and c-Rel (Figure 1A, B and S1B, C). There was a graded reduction in the frequency and number of FoxP3^{+} Treg cells upon deletion of *Rel*, *Rela*, or both. This demonstrated unique and partially redundant functions of both canonical NF-κB subunits in the development of Treg progenitors.

To assess whether NF-κB activation was required for the transition of Treg progenitors to FoxP3^{+} Treg cells, we isolated Treg progenitors and induced deletion of NF-κB subunits *in*

vitro using TAT-CRE protein (Joshi et al., 2002; Lio and Hsieh, 2008). We observed a 3-fold reduction in Treg frequency in cells lacking *Rel*, or both *Rela* and *Rel* (Figure 1C and data not shown). Hence these results suggested an intrinsic, specific and non-redundant role for canonical NF-κB subunits in the specification of FoxP3⁻ Treg precursors and in the expression of FoxP3. Moreover, deletion of *Rela* alone led to a modest, but statistically significant, decrease in the proportion and numbers of Treg cells in both spleen and lymph nodes (LN), but not in other tissues (Figure 1D–F and S1D). Mice lacking *Rel* exhibited a dramatic decrease in Tregs frequency in all tissues. This was further amplified by the deletion of both p65 and c-Rel, demonstrating a partially redundant role of both NF-κB subunits in homeostasis of peripheral Treg cells. Finally, we assessed the potential role of each NF-κB subunit in iTreg induction *in vitro*. Upon stimulation with Interleukin 2 (IL-2) and Transforming Growth Factor-Beta (TGF-β), cells lacking *Rela* gave rise to normal proportions of FoxP3⁺ cells (Figure 1G). Naïve T cells lacking *Rel* exhibited a partial defect in iTreg induction that was rescued by increasing doses of TGFβ. However, full ablation of the NF-κB canonical pathway, by deletion of both *Rela* and *Rel*, almost completely abolished the *in vitro* differentiation of naïve T cells into iTreg cells. These results suggested that, although p65 and c-Rel partially compensated for one another, they also played discrete roles in multiple steps of both nTreg and iTreg development.

Treg-specific deletion of c-Rel leads to a late and mild inflammatory phenotype

To bypass the block imposed by loss of NF-κB on Treg development and assess the role of NF-κB subunits in the homeostasis and function of mature Treg cells, we deleted *Rel* in Tregs, but not Tconv cells, using the *Foxp3*^YFP-cre deleter strain (Figure S2A). We did not observe early lethality or systemic inflammation (Figure 2A and data not shown) in *Foxp3*^YFP-cre*Rel*^f/f mice. Although 6–8 week-old *Foxp3*^YFP-cre*Rel*^f/f mice did not show any overt signs of illness, lung and liver histology revealed a modest increase in lymphocyte infiltration relative to the WT controls (Figure 2B). Moreover, the cellularity of the peripheral LN, but not the spleen, was significantly increased (Figure 2C). The percentage and number of activated CD4⁺ and CD8⁺ T cells were similar between WT and *Foxp3*^YFP-cre*Rel*^f/f mice in spleen (Figure 2D–F), but there was a mild increase in CD8⁺ T cell activation in LN (Figure S2B). We observed a trend toward increased production of IL-17 and Interferon (IFN)- by splenic CD4⁺ T cells in *Foxp3*^YFP-cre*Rel*^f/f mice (Figure 2G, H). Also, production of IFNγ, but not IL-17, by CD4⁺ T cells in the colon lamina propria and skin was increased in *Rel*-deficient mice (Figure S2E, F). The proportion and number of Treg cells were unaffected by the absence of c-Rel (Figure 2I, J and S2C). This data showed that c-Rel in Tregs was mostly dispensable for the maintenance of immune tolerance despite its crucial role in thymic Treg development.

Although aged *Foxp3*^YFP-cre*Rel*^f/f mice did not exhibit any obvious morbidity, 8-month old mutant mice showed overt splenomegaly and lymphadenopathy (data not shown), and liver and lung histology revealed increased lymphocytic infiltrates (Figure S2G). We also observed an increase in the frequency of effector T cells with a skewing towards IFNγ secreting T helper 1 (Th1) cells in spleen and LN (Figure S2H). Finally, we tested the suppressive function of c-Rel deficient Treg in T cell transfer-induced colitis, in which naïve Tconv cells were transferred to *Rag1*⁻/⁻ recipients alone or with WT or mutant Tregs. In

contrast with WT Tregs, *Rel*-deficient cells were completely unable to protect the recipient animals from weight loss or intestinal pathology (Figure 2K, L) suggesting a role for c-Rel in Treg suppressive function. Taken together, this data showed that c-Rel was largely dispensable for maintenance of immune tolerance but was important for regulation of Treg function in lymphopenic hosts.

Mice with Treg specific deletion of NF-κB p65 develop a severe inflammatory phenotype

To assess the potential role of p65 in Tregs, we crossed *Rela*-floxed mice with *Foxp3*[YFP-cre] mice, which resulted in selective loss of p65 in Treg, but not Tconv cells (Figure S3A). *Foxp3*[YFP-cre]*Rela*[f/f] mice were smaller than their WT littermates (data not shown) and showed accelerated mortality, with all mice dying between 5–15 weeks after birth (Figure 3A). This was associated with lymphoproliferative disease including splenomegaly and lymphadenopathy, as well as lymphocytic infiltration of lung and liver (Figure 3B, C and data not shown). Dorsal skin sections from *Foxp3*[YFP-cre] *Rela*[f/f] mice revealed hyperplastic epidermis and a robust immune cell infiltration with significant epidermal thickening (Figure S3B, C). Moreover, there was a dramatic increase in frequencies and numbers of CD4^{+} and CD8^{+} T cells secreting IFN-γ and with an activated/memory phenotype (Figure 3D–H and S3D).

Despite the lymphoproliferative disease, the proportion and number of Treg cells were in fact increased in secondary lymphoid tissues (Figure 3I, J and S3E). p65-deficient Tregs displayed normal expression of CD25 and Helios, which are important factors for Treg homeostasis (Figure S3F). This suggested a defect in the suppressive function of Tregs lacking p65. Tregs from *Foxp3*[YFP-cre]*Rela*[f/f] mice were able to suppress proliferation of Tconv cells *in vitro* (Figure S3G). However, *Rela*^{−/−} Treg cells were completely unable to rescue recipient mice from colitis in an *in vivo* suppression assay (Figure 3K, L). This, together with the increased production of IFNγ and IL-17 by CD4^{+} T cells in multiple tissues of *Foxp3*[YFP-cre]*Rela*[f/f] mice (Figure S3H, I), demonstrated that p65 is essential for Treg-dependent maintenance of immune tolerance.

Complete ablation of canonical NF-κB in Tregs leads to a *Scurfy*-like phenotype

Our results (Figure 1) suggested that c-Rel and p65 exhibited partially redundant functions, and therefore to test this prediction we generated *Foxp3*[YFP-cre]*Rela*[f/f]*Rel*[f/f] mice (Figure S4A). Consistent with our hypothesis, these mice showed a profound *Scurfy*-like phenotype with robust cutaneous inflammation and severe runting (data not shown). *Foxp3*[YFP-cre]*Rela*[f/f]*Rel*[f/f] mice died between 2 and 4 weeks after birth (Figure 4A) and demonstrated pronounced lymphocytic infiltration in lungs and liver (Figure 4B), as well as severe splenomegaly and lymphadenopathy (Figure 4C). *Foxp3*[YFP-cre]*Rela*[f/f]*Rel*[f/f] mice had significantly higher numbers and frequencies of CD44^{high} central and effector memory CD4^{+} and CD8^{+} T cells (Figure 4D–F and S4B)). There was also an increase in the number and frequency of CD4^{+} Tconv cells from *mutant* mice that produced IFNγ (Figure 4G, H). In addition, we also detected an increase in antibodies recognizing double stranded DNA (anti-dsDNA antibodies) in *Foxp3*[YFP-cre]*Rela*[f/f]*Rel*[f/f] mice (Figure S4E), similar to observations in *Scurfy* mice (Aschermann et al., 2013). Thus, canonical NF-κB in Treg cells is required for cellular and humoral tolerance.

This phenotype observed in $Foxp3^{\text{YFP-cre}}Rela^{\text{f/f}}Rel^{\text{f/f}}$ mice suggested a profound loss of Treg homeostasis. $Foxp3^{\text{YFP-cre}}Rela^{\text{f/f}}Rel^{\text{f/f}}$ mice had decreased Treg frequency in all examined tissues (Figure 4I, J and S4C). Also, the Mean Fluorescence Intensity (MFI) of Helios and CD25 was decreased in NF-κB-deficient Treg cells (Figure S4D). We next investigated whether those Treg cells were functional *in vivo*. In contrast to WT cells, $Rela^{-/-}Rel^{-/-}$ Tregs were completely unable to rescue $Rag1^{-/-}$ mice from colitis induced by transfer of WT CD4$^+$ Tconv cells (Figure 4K, L). Increased production of inflammatory cytokines in multiple tissues also confirmed the inability of *Rela-Rel*-deficient Treg cells to suppress effector and systemic inflammatory responses (Figure S4F, G). Thus, complete ablation of canonical NF-κB signaling impairs Treg homeostasis and function. This highlighted the crucial role of the canonical NF-κB pathway in the maintenance of immune tolerance.

Canonical NF-κB maintains the function and identity of mature Treg cells

We next investigated whether NF-κB was continuously required for mature Treg function. We induced conditional deletion of p65 and c-Rel in peripheral Tregs by administrating tamoxifen to Rela- and Rel-floxed mice crossed with $Foxp3^{\text{eGFP-Cre-ERT2}}xRosa26^{stop-eYFP}$ mice (Rubtsov et al., 2010) (Figure 5A). In these mice, all Tregs express Green Fluorescent Protein (GFP), but tamoxifen treatment induces expression of Cre and Yellow Fluorescent Protein (YFP), allowing isolation of NF-κB deleted Treg cells by flow cytometry. We assessed Treg frequency seven days after initiating tamoxifen treatment. The percentages of FoxP3$^+$ Tregs were significantly reduced upon deletion of *Rel* and *Rel*+*Rela* (Figure 5B), suggesting that NF-κB played a role in the maintenance of Tregs or Treg identity. Moreover, the MFI of staining for FoxP3, as well as CD25 and GITR, was decreased in Tregs following inducible deletion of *Rel* or both *Rel* and *Rela*, but not in cells in which only *Rela* was deleted (Figure 5C). We also observed a loss of *Foxp3* mRNA expression in *Rel*+*Rela* deleted cells (Figure 5D). These data suggested that canonical NF-κB activity and, in particular c-Rel, was essential for the maintenance of the mature Treg population. We next tested the *in vivo* suppressive function of Treg cells with inducible deletion of *Rel* and *Rela* (induced-double knockout, iDKO Treg). Similar to $Foxp3^{\text{YFP-cre}}Rela^{\text{f/f}}Rel^{\text{f/f}}$ Tregs, iDKO (TMX-$Foxp3^{\text{eGFP-Cre-ERT2}}$Rosa26$^{stop-eYFP}Rela^{\text{f/f}}Rel^{\text{f/f}}$) Tregs failed to prevent development of colitis in $Rag1^{-/-}$ mice (Figure 5E, F). This data established an essential role for NF-κB in Treg function *in vivo* and suggested the canonical NF-κB pathway may play an important role in the maintenance of Treg identity.

Canonical NF-κB maintains the Treg transcriptome

The finding that NF-κB was required for Treg suppressive function is consistent with NF-κB being a key mediator of transcriptional events downstream of TCR ligation. However, it is unclear how NF-κB fulfills this role in both Treg and Tconv cells. Our finding that loss of canonical NF-κB in Tregs resulted in a loss of Treg function led us to hypothesize that NF-κB controls a distinct, lineage specific, transcriptional program in Treg cells. To delineate the NF-κB-dependent transcriptomes in Tregs we used high-throughput RNA-sequencing (RNAseq) analysis to compare the global gene expression patterns between Tregs of various genotypes and WT Tconv cells stimulated or not with anti-CD3 and anti-CD28. Unsupervised hierarchical clustering (Figure 6A) of the data by genotype indicated a

profound effect of NF-κB on the Treg transcriptome. As expected, based on the disease phenotype observed, single deletions of *Rela* or *Rel* induced largely distinct perturbations in gene expression. *Rela*$^{-/-}$*Rel*$^{-/-}$ Tregs were distinct from WT Tregs, *Rela*$^{-/-}$ and *Rel*$^{-/-}$ Tregs, clustering as an outlier group. Furthermore, we found that stimulated and unstimulated Tregs clustered together, segregating by genotype rather than by presence or absence of stimulation. When additional published Treg and Tconv datasets were included in clustering (Wakamatsu et al., 2013), *Rela*$^{-/-}$*Rel*$^{-/-}$ Tregs clustered together with WT Tconv cells, emphasizing the loss of Treg signature gene expression upon NF-κB deletion (Figure S5A). The distinct set of genes in *Rela*$^{-/-}$*Rel*$^{-/-}$ containing loss of Treg signature genes was also observed in the clustering of our RNAseq dataset without public data, using the genes with ANOVA fold change higher than 1 (P < 0.05) (Figure S5B). Principal component (PC) analysis confirmed that *Rela*$^{-/-}$*Rel*$^{-/-}$ Tregs exhibit a distinct transcriptome in comparison to either single knockout or WT Tregs (Figure S5C). While the first PC, accounting for 32.9% of the variance, established *Rela*$^{-/-}$*Rel*$^{-/-}$ Tregs as having a divergent transcriptional profile, PC2 and PC3, together accounting for 31.2% of the variance, emphasized the transcriptional similarity between *Rela*$^{-/-}$*Rel*$^{-/-}$ Treg and Tconv cells (Figure S5C). Consistent with both the PC analysis and clustering, we found that gene expression was equally impaired in unstimulated and stimulated *Rela*$^{-/-}$*Rel*$^{-/-}$ Tregs (Figure 6B).

Although NF-κB can both activate and repress gene expression, c-Rel and p65 are generally considered positive regulators of transcription. However, almost equal numbers of genes were up- and down-regulated upon loss of these NF-κB subunits in Tregs (Figure 6C). We also found that the majority of genes differentially expressed in *Rela*$^{-/-}$*Rel*$^{-/-}$ vs WT Tregs cells were not significantly altered in either *Rel* or *Rela*-deficient Tregs (Figure 6C). This, together with the partial phenotypic overlap resulting from Treg specific gene deletion (Figures 2 and 3), suggested considerable compensation between p65 and c-Rel. We found that numerous Treg signature genes were downregulated, and conversely expression of inflammatory cytokine transcripts increased, in *Rela*$^{-/-}$*Rel*$^{-/-}$ Tregs compared to WT Tregs in both stimulated and unstimulated cells (Figure 6B, D). In particular, the expression of *Ifng*, *Il17a*, *Il2*, *Il4* and *Il13* was increased at the mRNA and protein levels in *Rela*$^{-/-}$*Rel*$^{-/-}$ Tregs (Figure 6E, S5F). Gene set enrichment analysis (GSEA) revealed significant enrichment of Treg genes as well as chemokine, cytokine and transcription factor genes (Figure S5E). Within the Treg gene set, expression of *Foxp3* as well as two transcription factors that act cooperatively with FoxP3, *Ikzf2* (Helios) and *Ikzf4* (Eos) were reduced in Tregs from *Foxp3*$^{YFP-cre}$*Rela*$^{f/f}$*Rel*$^{f/f}$ mice (Figure 6D, left panel, and S5F). Similarly, the Treg signature genes, *Cd83*, *Gpr83* and *Lrrc32* (GARP), were also downregulated in *Rela*$^{-/-}$*Rel*$^{-/-}$ Tregs. Additional genes implicated in Treg homeostasis that were significantly altered in *Rela*$^{-/-}$*Rel*$^{-/-}$ Tregs included chemokines and chemokine receptors, e.g. *Ccr7* and *Ccr6* (Figure S5E). These results suggested that deficiencies in Treg localization and recruitment may potentially explain why the defect in function of Treg lacking NF-κB manifested *in vivo,* but not *in vitro*. We also noted that several cytokines such as *Il22*, *Il4* and *Il13*, which are not expressed in WT Treg cells, were upregulated in *Rela*$^{-/-}$*Rel*$^{-/-}$ Tregs and further increased upon TCR stimulation (Figure 6B, D and Figure S5D–F) As expression of *Foxp3* was down-regulated in *Rela*$^{-/-}$*Rel*$^{-/-}$ Treg cells, we also assessed whether the impairment of *Rela*$^{-/-}$*Rel*$^{-/-}$ Treg transcriptome could be the consequence of FoxP3 loss

rather than a direct effect of NF-κB ablation. Comparison of FoxP3-dependent genes (Gavin et al., 2007) with $Rela^{-/-}Rel^{-/-}$ -affected genes revealed only a partial overlap (Figure S5G). While some prototypic Treg genes with decreased expression in $Rela^{-/-}Rel^{-/-}$ Tregs, such as $Ctla4$ or $Ikzf2$, were FoxP3-dependent, GSEA of the 2653 $Rela^{-/-}Rel^{-/-}$ -affected FoxP3-independent genes also highlighted a loss of the Treg signature (Figure S5H). Thus, ablation of NF-κB led to a loss of Treg identity not only indirectly through the down-regulation of FoxP3 expression but also by directly affecting expression of NF-κB-dependent genes. As $Foxp3^{YFP-cre}Rela^{f/f}Rel^{f/f}$ mice develop an early systemic inflammatory syndrome, we then asked whether the altered gene expression in $Rela^{-/-}Rel^{-/-}$ Tregs was due to the intrinsic absence of NF-κB in the cells, or due to inflammatory cytokines in the local environment. The modest but significant increase of the expression of $Ifng$, $Il5$ and $Il22$ in Rel-deficient Tregs was a first indication that loss of NF-κB subunits led towards a Teff-like phenotype independent of local inflammation as young $Foxp3^{YFP-cre}Rel^{f/f}$ mice do not display any autoimmune phenotype (Figure 2). To further analyze the effect of NF-κB-ablation independently of the local milieu, we deleted floxed $Rela$ and Rel $in\ vitro$, using TAT-Cre. Gene expression patterns of control and iDKO Tregs were then compared by RNAseq. As observed upon $in\ vivo$ deletion of NF-κB, iDKO Tregs exhibited increased expression of various inflammatory cytokines such as $Il17a$, $Il22$, $Ifng$ and $Il4$ (Figure 6F). Moreover, some hallmarks of Treg identity, such as $Foxp3$, $Cd83$ and $Id3$, were also down-regulated. This demonstrated that NF-κB exerts a cell-intrinsic effect to maintain Treg identity and prevent the expression of Tconv-specific genes. Taken together, this analysis suggested that NF-κB regulates distinct transcriptional programs in Treg and Tconv cells and demonstrated an important role for NF-κB in maintenance of a lineage specific transcriptome in Tregs.

NF-κB p65 directly coordinated the expression of Treg-signature genes

To characterize lineage specific, differential DNA binding patterns by NF-κB in Treg and Tconv cells, we used chromatin immunoprecipitation with massively parallel DNA sequencing (ChIPseq). After identifying putative p65 occupancy sites using the Irreproducible Disovery Rate (IDR) framework (Li, 2011) as outlined by ENCODE, we compared the number of peaks between populations. A fraction of peaks were detected both with and without stimulation, and these were mostly overlapping between Treg and Tconv (Figure 7A). To define a more rigorous set of overlapping regions putatively bound by p65 across all four conditions, we identified peaks in stimulated Treg cells that were also observed in stimulated Tconv cells, as well as in both unstimulated Treg and Tconv cells. We named this subset of 1571 peaks associated with 1297 genes "constitutive" because of the relatively high enrichment compared to input across all 4 samples (Figure 7B). GSEA on these "constitutive" p65-bound genes showed genes such as cell cycle-related genes (e.g. $Cdk4$ and $Birc5$) (Figure S6A). Interestingly, at a number of peaks, binding intensity was strongly increased upon stimulation in both Tconv and Treg similarly, confirming that NF-κB activation and binding to chromatin is induced upon TCR+CD28 signaling (Figure 7A, B). We defined a set of shared peaks in both Treg and Tconv stimulated cells that were also differentially enriched in stimulated versus unstimulated Treg cells, but not significantly differentially occupied between Treg and Tconv (see Methods). We named this subset "Treg-Tcon shared" and found that this gene set corresponding to 3552 genes was enriched for genes such as cytokines and cytokine receptors, e.g Tnf, as well as known NF-κB-induced

genes such as *Nfkbia* (IκBα) (Figure S6B). We also detected a number of peaks that were significantly higher in stimulated Treg compared to Tconv. This final set of p65 peaks specific to stimulated Treg cells was defined by identifying stimulated Treg binding sites differentially enriched over both unstimulated Treg and stimulated Tconv cells. Of the 432 genes putatively associated with these 859 peaks, several fall within the well-described set of Treg signature genes such as *Foxp3*, *Ikzf2* and *Lrrc32* (Figure 7F). GSEA of this "Treg-stim enriched" population was enriched in genes highly expressed in Treg versus Tconv (Figure S6C). Only a few peaks were specifically detected in stimulated Tconv but not Treg cells, suggesting that p65 binding could be influenced by a Treg-specific environment that does not exist in a Tconv-specific landscape. The distribution of peak distances from the nearest transcription start site (TSS) and the distribution of genomic annotations associated with those peaks showed significant variation between different samples (Figure S6D). In contrast with constitutive peaks, Treg stim-enriched peaks showed marked increase in the fraction of peaks located in distal intergenic regions, suggesting that they might be binding to putative enhancers. These peaks contributed to the overall increase in Treg stim peaks (Figure 7A). Our data demonstrated that TCR+CD28-induced NF-κB binding is different in Treg and Tconv, suggesting that the Treg-lineage environment influences NF-κB binding and function.

We next looked for p65 binding motif enrichment in each gene subset using SeqGL (Setty and Leslie, 2015), as described in Methods. We found an enrichment for a Rel Homology domain-like motif nearby both Treg stim-enriched and Treg-Tcon shared summits (Figure 7C). The peaks shared by Tconv and Treg were enriched with motifs for various transcription factors such as CREB, ETS and RUNX1 in addition to NF-κB REL-binding motifs (Figure 7C). On the other hand, Treg-enriched peaks were predominantly enriched only with REL-binding motifs. This suggests that preferential binding of p65 to those sites in Treg over Tconv may not be due to unique unconventional binding motifs.

We then analyzed whether Treg-specific p65-binding could simply rely on a differential chromatin accessibility in Treg and Tconv cells. DNase hypersensitivity (HS) experiments have previously demonstrated a discrete chromatin accessibility in Treg and Tconv (Samstein et al., 2012). To assess a possible role for accessibility in p65-binding, we aligned their DNase HS sequencing data in Treg and Tconv cells to our p65 ChIPseq dataset. Interestingly, in Treg-enriched peaks, chromatin accessibility was significantly higher in Treg versus Tconv, whereas the opposite trend was observed in Treg-Tconv shared peaks (Figure 7D). This was illustrated by higher DNase HS signals in Treg at numerous Treg-associated genes, such as *Foxp3*, *Ikzf2* or *Lrrc32* (Figure 7G). Similar results were obtained when using a recently reported (Kitagawa et al., 2017) ATAC-Seq dataset (Figure 7E). This correlation suggests that chromatin accessibility yields increased p65 binding at Treg-enriched loci, resulting NF-κB-dependent regulation of the Treg specific transcriptional program.

To further elucidate the direct contribution of p65 binding to the differential gene expression of Tconv and Treg cells, we next focused our analysis on Treg and Tconv specific genes. We first defined a set of 587 "Treg signature" genes whose expression was significantly higher in WT Treg than WT Tconv, based on public datasets (Ye et al., 2014) (Figure 7F). As a

counterpart, we used a "Tconv signature" set composed of 211 genes, as well as the total coding genome. We assessed the potential association between p65 binding at Treg-stim enriched, Treg-Tcon shared and constitutive peaks, FoxP3 binding peaks (Samstein et al., 2012), Tconv—Treg and Treg $Rela^{-/-}Rel^{-/-}$ —WT differentially expressed genes, and Tconv—Treg signature genes. We found a strong enrichment of Treg-specific p65 binding in Treg-signature genes. Expression of many of these genes was dependent on NF-κB, as their expression was down-regulated in $Rela^{-/-}Rel^{-/-}$ Tregs (Figure 7F). Interestingly, the fraction of genes bound by both FoxP3 and p65 was higher in Treg-signature genes than in the rest of the genome (Figure 7F and S6E), further underlining the importance of these transcription factors in Treg-specific gene expression. This was illustrated by FoxP3 binding in the vicinity of p65 binding at *Foxp3*, *Ikzf2* and *Lrrc32* loci (Figure 7G). Taken together, our results showed that NF-κB directly directed the expression of Treg-essential genes by accessing specific, open loci in Treg cells.

DISCUSSION

Even though Tconv and Treg cells develop from the same pool of thymocyte progenitor cells, they have diametrically opposed functions in the immune system. Consistent with their common developmental lineage, Treg and Tconv cells share many of the same cell surface receptors and intracellular signaling pathways. This common nature of T cell signaling events in both Treg and Tconv cell represents a significant barrier to the development of immunomodulatory therapies. Thus, targeting of a common signaling mechanism in both cell types may result in a single agent simultaneously promoting and inhibiting Tconv responses. Given the importance of Tregs in both beneficial peripheral tolerance and detrimental tumor tolerance, it is therefore essential that we understand how the same TCR signaling leads to such different biological functions in Treg and Tconv cells.

It has been proposed that activation of the canonical NF-κB pathway upon TCR and CD28 triggering is important for normal Treg differentiation. For instance, mice lacking any member of the CARMA-1-Bcl-10-Malt1 complex exhibit a profound lack of FoxP3^{+} thymocytes (Molinero et al., 2009), whereas constitutive activation of NF-κB through an IKKEE transgene in T cells increases thymic Treg cells (Long et al., 2009). Furthermore, germline deletion of c-Rel leads to reduced transition into the Treg progenitor step and subsequent maturation into FoxP3^{+} Treg cells (Grigoriadis et al., 2011; Isomura et al., 2009). However, deletion of *Rel* does not fully eliminate Treg cells, leaving unclear the role of the canonical NF-κB pathway. The study of $Rela^{-/-}$ mice was complicated by the embryonic lethality of these mice although indirect evidence pointed towards a role for p65 in FoxP3 expression (Deenick et al., 2010; Isomura et al., 2009; Soligo et al., 2011). In the current study, we demonstrated a crucial requirement for both canonical NF-κB subunits in the generation of FoxP3^{−} Treg precursors. Canonical NF-κB signaling, along with IL-2 to STAT-5 and IκB-NS signals (Lio and Hsieh, 2008; Schuster et al., 2012), is crucial for the subsequent expression of FoxP3 and for mature Treg homeostasis in secondary lymphoid organs. We also showed a partial redundancy as absence of both p65 and c-Rel led to nearly complete abolishment of Treg cells in the thymus and the periphery.

To date, only a moderate role for NF-κB was previously described in the *in vitro* iTreg polarization (Jana et al., 2009; Visekruna et al.). Here we showed that naïve T cells fully lacking canonical NF-κB were unable to give rise to iTreg, even in the presence of exogenous IL-2, while deletion of only *Rela* or *Rel* had nearly no effect. Thus, our studies demonstrated a redundant but crucial role for canonical NF-κB activity in iTreg development and highlighted a specific role for each NF-κB subunit in Treg development *in vivo* and *in vitro*.

To examine the role of NF-κB in Tregs more precisely, we performed Treg-specific conditional deletion of *Rela* and/or *Rel*. The profound autoimmunity observed upon deletion of *Rela* in Tregs was consistent with recently reported results (Messina et al., 2016). However, these mouse models showed that both p65 and c-Rel played essential, although partially redundant, roles in the function of Treg cells. In contrast to its essential role in Treg development, we observed little effect of *Rel* deletion on the ability of Tregs to suppress systemic lymphoproliferative disease. In contrast, mice in which both subunits are deleted in Treg cells display a *Scurfy*-like phenotype with severe lethal lymphoproliferative and autoimmune disease despite only modest reductions in Treg numbers. Therefore, canonical NF-κB is essential for the function of both Treg and Tconv cells.

The graded phenotype observed in mice lacking c-Rel, p65, or both NF-κB subunits in Treg offers some hints as to the relative importance of specific canonical NF-κB regulated genes in Treg function. That is, while *Foxp3*[YFP-cre]*Rela*[f/f]*Rel*[f/f] mice exhibit a *Scurfy*-like phenotype, mice lacking *Rela* in Tregs display a relatively delayed, though still severe phenotype, while mice lacking only *Rel* in Tregs show a substantially delayed and mild phenotype. Thus, it might be expected that an analysis of gene expression between genotypes would be instructive in understanding the basis of this graded phenotype. Although expression of specific candidate genes known to be important for Treg function were clearly altered, it seemed that graded changes in expression of several target genes, likely due to partial compensation between canonical NF-κB subunits, accounted for the difference in Treg suppressive phenotypes observed. When the canonical NF-κB pathway was completely ablated in Treg cells by deleting both *Rela* and *Rel*, Tregs not only lost suppressive function and their expression of Treg-signature genes but also upregulated the expression of certain Tconv genes, especially inflammatory cytokines. This was due to a specific function of c-Rel, as *Rel*-deficient Tregs, but not *Rela*-deficient Tregs, displayed increased expression of *Ifng* among the cytokines. These data suggested that in Tregs, c-Rel, specifically, was essential for the suppression of effector cytokine expression. Further analysis of the functions of c-Rel and p65 in Tregs demonstrated a unique role for c-Rel in activated Treg function and maintenance of tumor tolerance (*Grinberg-Bleyer et al., 2017*). Overall, canonical NF-κB regulated a lineage specific transcriptome comprising of multiple genes with a broad role in the maintenance of Treg identity and function, which suppressed a conventional CD4^{+} T cell phenotype in Tregs.

While canonical NF-κB is well-known to be critical for effector cell differentiation and expression of inflammatory cytokines in Tconv cells, our findings indicate that the same signaling pathway regulated a dissimilar lineage defining transcriptional program in Treg cells. Thus, the canonical NF-κB pathway, in both cases activated through ligation of the

same TCR complex, activated a qualitatively and quantitatively distinct transcriptional program with opposing biological functions. Two potential mechanisms help explain the divergent role of canonical NF-κB in Treg and Tconv cells: the extent of NF-κB activation and access to κB DNA binding sites. Tregs depend on constitutive TCR signaling for maintenance of suppressive function (Levine et al., 2014). Thus, we, like others (Messina et al., 2016), saw higher levels of nuclear canonical NF-κB subunits in circulating Tregs compared to Tconv cells, consistent with an ongoing role for NF-κB in the regulation of the Treg specific transcriptome (data not shown). However, increased canonical NF-κB activation in Tregs compared with Tconv cells did not account for the divergent transcriptional programs regulated by NF-κB in the two cell types. TCR ligation induced equivalently robust canonical pathway activation in both cell types, yet NF-κB regulated distinct sets of genes in Treg and Tconv cells. This suggested that changes in the chromatin landscape in Treg cells might be a major determinant of Treg identity. Consistent with this idea, NF-κB p65 ChIP-seq identified substantial differences in chromatin binding between Treg and Tconv cells, following TCR stimulation. In particular, the number and intensity of many peaks were higher in Treg cells compared to Tconv cells. These Treg-enriched peaks were often found in Treg-associated genes, such as *Foxp3* or *Ikzf2*, further confirming a direct Treg-lineage specific role for NF-κB. This specific binding was not due to an altered binding motif. However, DNase-seq and ATAC-seq analyses revealed greater chromatin accessibility in Treg than Tconv cells at these loci. This suggested that lineage-associated p65-binding relied on a Treg-specific chromatin structure rather than on a specific DNA sequence.

The molecular mechanism driving distinct p65 binding in Treg cells remains to be elucidated. A possibility is that other Treg-specific transcription factors may drive NF-κB activity, or cooperate with p65, to regulate Treg gene expression. Given that FoxP3 is the lineage specific transcription factor that differentiates Treg and Tconv cells, it is possible that FoxP3 itself coordinates Treg-specific p65-binding and activity. It was previously suggested that FoxP3 and p65 may influence NF-κB activity, for instance on the *GITR* locus (Tone et al., 2014). Analysis of our ChIPseq and public data showed binding for both p65 and Foxp3 on multiple Treg genes, including *Foxp3* itself, *Ikzf2*, *Lrrc32* or *Ctla4*. Other transcription factors, such as Foxo1/3 or ETS-1, were also suggested to influence the expression of NF-κB-dependent Treg signature genes (Kerdiles et al., 2010; Ouyang et al.; Samstein et al., 2012). This suggests that other lineage specific factors likely also contributed to the lineage-specific transcriptional program regulated by canonical NF-κB. Understanding how different chromatin modifying and transcription factors orchestrate the establishment of a Treg-specific transcriptome would be of great interest.

In summary, our studies demonstrated an absolute requirement for canonical NF-κB for regulatory T cell function *in vivo*. Given the known roles of canonical NF-κB in conventional T cell responses, these data suggested that considerable caution is need for the development of immunomodulatory therapeutics that target the NF-κB pathway. In this regard, the differential roles of p65 and c-Rel in Tregs, identified here, as well as in B and T cell immune responses, previously described, suggest that approaches that selectively target specific components of the NF-κB signaling pathway may have greater utility compared to inhibitors that shut down the entire pathway, e.g. inhibitors that target IKK. Finally, these

studies demonstrated an intriguing functional plasticity for the NF-κB pathway where even within closely related cellular lineages, the same NF-κB subunits could regulate highly divergent transcriptional programs with profound biological ramifications.

STAR Methods

CONTACT FOR REAGENT AND RESCOURCE SHARING

Further information and requests for resources and reagents should be directed to and will be fulfilled by the Lead Contact, Sankar Ghosh (sg2715@cumc.columbia.edu).

EXPERIMENTAL MODELS

Mice—*Rela*$^{f/f}$ mice were obtained from Roland Schmid (Munich, Germany) (Algul et al., 2007) and *Rel*$^{f/f}$ mice from Ulf Klein (Columbia University, New York)(Heise et al., 2014). *FoxP3*^{cre} mice were originally purchased from Jackson laboratory. *FoxP3*$^{eGFP-Cre-ERT2}$ x *Rosa26*$^{stop-eYFP}$ mice were obtained from A. Rudensky and crossed with *Rela*$^{f/f}$ and *Rel*$^{f/f}$ mice. All the mice were bred in the specific-pathogen-free (SPF) facility at Columbia University (New York, NY). *Rag1*$^{-/-}$ mice were originally purchased from Jackson laboratory and bred and maintained at our animal facility. 5–8 weeks-old male or female mice were used for most of experiments but 18–28 days-old mice were used to analyze *FoxP3*^{cre}*Rela*$^{f/f}$*Rel*$^{f/f}$ mice due to their early mortality. To analyze old *FoxP3*^{cre}*Rel*$^{f/f}$ mice, 7–8 months mice were used. All experiments were performed following the animal protocol approved by Institutional Animal Care and Use Committee of Columbia University (protocol AAAI 4700).

METHOD DETAILS

Cell Isolation—Cells were isolated from spleens and lymph nodes by grinding with cell strainers. For isolation of cells from the intestine, colons were collected and cut into small pieces after being cleaned up. Intestinal pieces were incubated in PBS containing 5 mM EDTA and 10 mM HEPES at 37°C with shaking for 20 minutes twice to acquire intestinal epithelial cells. Remaining pieces were digested with culture media containing 1 mg/ml collagenase type IV (Sigma) and 1mg/ml DNase I (Sigma) at 37°C for 15 minutes twice to acquire lamina propria cells. Lymphocytes were isolated by Percoll gradient from isolated cells. For isolation of cells from lungs, lungs were cut into small pieces and digested in culture media containing Collagenase and DNase I at 37°C. Then, digested lung fragments were passed through cell strainers to get single cell suspensions. Lymphocytes were isolated by Percoll gradient.

Flow Cytometry and Sorting—Isolated cells were stained with αCD4, αCD8, αCD3, αTCRβ, αCD44, αCD62L, αFoxP3, αIL-17 and αIFN-γ (eBioscience and Tombo). For FoxP3 and cytokine staining, cells were stained according to the manufacturer's protocol form FoxP3 staining kit (Affimetrix/eBioscience). For cytokine staining, cells were stimulated with 50 ng/ml PMA and 1 μg/ml ionomycin in the presence of GolgiPlug (BD Bioscience) for 4 hours at 37°C and stained for surface markers followed by fixation/ permeabilization and staining for cytokines. Stained cells were acquired with LSRII or LSR Fortessa cytometers; data was analyzed using FlowJo (Treestar) (BD Bioscience). For

sorting of Treg cells, CD4+ T cells were enriched by using mouse CD4+ T cell isolation kit (Miltenyi) or Magnisort mouse CD4+ T cell enrichment kit (Affimetrix/eBioscience) and then cells were sorted by FACSAria (BD Bioscience).

In vitro Treg differentiation—CD4$^+$CD44^{low}CD25$^-$ naïve T cells were FACS-sorted from splenocytes suspensions. 10^5 T cells were cultured in complete RPMI (Gibco) with 10^5 T-cell depleted, mitomycin C-treated WT splenocytes and 2.5 µg/mL anti-mCD3 (BioXCell), in the presence of 10 ng/mL mIL-2 (Peprotech) and grading doses of human TGF-β1 (Peprotech), for 4 days at 37C. Cells were then stained for flow cytometry analysis.

Western Blotting—Total lysates were extracted using RIPA buffer and protease inhibitors with SDS. 20 µg protein extracts were resolved in polyacrylamide gels and transferred onto PVDF membranes. Membranes were incubated with anti-p65, c-Rel (Santa-Cruz) and GAPDH (Fitzgerald) Abs, followed HRP-coupled secondary Abs.

In Vivo Suppression Assay—Tconv cells were sorted from wild type mice and Treg cells were sorted from wildtype or conditional knockout mice. 4×10^5 Tconv cells were transferred to RAG1 mice by i.v. injection together with wild type or knockout Treg cells (1×10^5). Tconv cells were also transferred without Treg cells as a control group. Weight was monitored weekly after adoptive transfer to observe progression of disease. Mice were euthanized when some of them reached 20% reduction of initial weight, and colons and other lymphoid organs were collected for H&E staining and flow cytometric analyses.

In Vitro Suppression Assay—Tconv cells were sorted from wildtype mice and Treg cells were sorted from wildtype or conditional knockout mice. Tconv and Treg cells were co-cultured at different ratios of Tconv:Treg in the presence of anti-CD3 and anti-CD28 antibodies. Tconv cells were also cultured without Treg cells as a control. Cells were cultured for 3 days and 1 µCi of ^{3}H-thymidine was added to each well 8 hours before harvest. T cell proliferation was observed by measuring the incorporation of ^{3}H-thymidine by the scintillation counter.

Quantitative RT-PCR (qRT-PCR)—RNA was prepared from cells by using RNeasy Mini Kit or RNeasy Plus Mirco Kit (Qiagen). cDNAs were synthesized by using SuperScript III (Invitrogen) and quantitative PCR was performed by using SYBR Green (Quanta Biosciences) using a CFX96 or CFX384 Thermal Cycler (BioRad). Expression level was normalized by GAPDH or tubulin.

Inducible deletion of genes by tat-cre treatment—Cells were resuspended in ADCF-Mab serum free media (HyClone) and Tat-cre (Protein and Proteomics Core Facility, The Children's Hospital of Philadelphia) was also diluted in ADCF-Mab media to 100 µg/ml concentration. Cell suspension and Tat-cre solution were prewarmed for 10 minutes at 37°C and then mixed at a 1:1 ratio. Mixture of cells and Tat-cre was incubated for 45 minutes at 37°C. Transduction was stopped by adding growth media containing 10% FCS. Cells were washed again with growth media containing 10% FCS and returned to culture.

Inducible deletion of genes by tamoxifen treatment—Tamoxifen in corn oil was administered by *i.p.* injection three consecutive days with 4 mg per mouse. After one week, mice were euthanized and cells with deletion were isolated by FACS based on expression of YFP from tamoxifen-inducible ROSA-floxed system. Isolated cells were then used for further experiments.

Histology—Mouse tissues were fixed in 10% formalin and stored in 70% ethanol until staining. All the fixed tissues were embedded in paraffin, sliced and stained by H&E in Histology Core at Columbia University Medical Center. Disease severity score was determined by severity of immune cell infiltration: >4 (most severe), 2 to 3 (severe), 1 (mild), and 0 (none). For ears, thickness of ear skin was measured after taking photos of H&E staining in AxioVision software.

RNAseq—Tconv and Treg cells were sorted from various mouse strains and stimulated with 5 μg/ml plate-bound anti-CD3 and 1 μg/ml anti-CD28 antibodies for three hours in the presence of IL-2 (Peprotech). 2 ng/ml IL-2 was added to Tconv culture and 10 ng/ml IL-2 was added to Treg culture. Cells were harvested and RNA samples were prepared. Quantity and quality of RNA samples were measured by Bioanalyzer (Molecular Pathology core at Herbert Irving Comprehensive Cancer Center, Columbia University). Library construction and sequencing were done by Columbia Genome Center. Poly-A pull-down was used to enrich mRNAs from total RNA samples and libraries were prepared by using Illumina TruSeq RNA prep kit. Libraries were then sequenced using Illumina HiSeq2000. All the RNAseq analyses except one set (paired-end 60 million reads) were single-end 30 million reads.

Chromatin immunoprecipitation (ChIP) assay for sequencing—T cells were fixed with 1% formaldehyde (Sigma) for 10 minutes at room temperature, quenched with 0.125 M glycine for 10 minutes and then washed in PBS. Fixed cells were lysed in Cell lysis buffer (25 mM HEPES pH 7.8, 1.5 mM $MgCl_2$, 10 mM KCl, 0.1% NP-40) with freshly added 1 mM DTT and protease inhibitors by incubating on ice for 10 minutes. Lysates were centrifuged at 5400 rpm for 5.5 min for nuclei isolation. Isolated nuclei were lysed in Nuclear lysis buffer. Nuclei lysates were sonicated by Bioruptor (Diagenode). Anti-p65 antibody (C-20, Santa Cruz Biotechnology) was incubated with Dynabeads™ protein A (Invitrogen) to prepare antibody-bound beads. Sonicated lysates were mixed with antibody-bound beads and immunoprecipitated overnight at 4°C. Beads were washed and incubated with RNase for 30 min at 37°C followed by incubation with proteinase K for 2 hours. Then, beads were decrosslinked overnight at 65°C and immunoprecipitated DNA fragments were isolated by QIAquick PCR purification kit (Qiagen). Small aliquots of DNA samples were used for qPCR to confirm the efficiency of ChIP reaction. The concentration of immunoprecipitated DNA and input DNA was determined by Bioanalyzer.

ChIP sequencing (Illumina)—Library preparation and sequencing were performed by Admera Health. Library was constructed on immunoprecipitated DNA according to manufacturer's recommendations (KAPA Hyper Prep Kit). Samples were enriched with PCR with 12 cycles (Eppendorf Mastercycler ep gradient S; Eppendorf AG, Hamburg,

Germany) with the program suggested on the commercial kit manual. Afterward, double size selection was performed with AMPure XP beads (Beckman Coulter, High Wycombe, UK) for a final library size of 500 bp. After pooling and denature, the samples were sequenced on the HiSeq with a 150 PE read length configuration.

Preliminary processing of sequencing data—Raw FASTQ reads were initially removed of adapter and low base quality contamination using Trim Galore! v0.4.1 (https://www.bioinformatics.babraham.ac.uk/projects/trim_galore/), which implements cutadapt(Martin, 2011) (http://cutadapt.readthedocs.io/en/stable/index.html) as the underlying base removal algorithm. Trimmed reads were subsequently aligned using BWA mem(H. Li and Durbin, 2009) (http://bio-bwa.sourceforge.net/). Post-alignment preprocessing was performed with the Picard suite of tools (http://broadinstitute.github.io/picard/), ' IndelRealigner' and ' MarkDuplicates' , and samtools(H. Li *et al.*, 2009) (http://samtools.sourceforge.net/). Aligned reads with non-zero mapping quality were retained in BAM format. Genome-wide coverage tracks were produced using the deepTools v2.3.6(Ramirez *et al.*, 2016) (http://deeptools.readthedocs.io/en/latest/#) ' bamCoverage' function with 50bp bins and an effective genome size of 2,451,960,000 bases and scaled to 1X coverage based on the number of reads mapped to autosomal chromosomes. Coverage was calculated from reads extended to estimate fragment size as determined by the cross-correlation analysis provided by the ' phantompeakqualtools' package(https://www.encodeproject.org/software/phantompeakqualtools/). Coverage signal was further summarized by taking the mean across replicates within groups. In the case of the public DNase I hypersensitivity data, mean coverage signal was additionally quantile normalized between Treg and Tconv cell types using the ' normalize.quantiles' function from the ' preprocessCore' R package. All signal and peak results were visualized in genomic context using the WashU EpiGnome Browser(Zhou *et al.*, 2011) (http://epigenomegateway.wustl.edu/).

Identification of regions of enrichment (peak-calling)—MACS v2.1.1.20160309(Yong Zhang *et al.*, 2008) (https://github.com/taoliu/MACS) was used for peak identification within the Irreproducible Discovery Rate (IDR) framework described by the ENCODE project(Q. Li *et al.*, 2011; Landt *et al.*, 2012) (https://sites.google.com/site/anshulkundaje/projects/idr) to produce a single consensus peak call set for each replicate group, using appropriate ChIP/input pairs when applicable. In brief, ' macs2 callpeak' at a permissive p-value threshold of 0.1 for various permutations of the replicate data, independent, combined, and in several pseudo-replicate combinations, to ascertain an appropriate threshold to make peaks calls utilizing the total combined replicate data. We chose to apply the more strict "conservative" threshold to identify our peak call sets.

Peak annotation—Consensus IDR peak calls were further characterized using the bedtools suite v2.25.0-24-g3d31735-dirty(Quinlan and Hall, 2010) (http://bedtools.readthedocs.io/en/latest/). For more rigorous peak comparisons, we employed the PePr algorithm(Yanxiao Zhang *et al.*, 2014) (https://github.com/shawnzhangyx/PePr) to identify significantly differential occupied or accessible regions. PePr models read counts using a negative binomial distribution with a dispersion parameter determined based on

proximal regions. Peak associations with genes and genomic feature classes (promoter, intron, exon, etc.) were determined using the ChIPseeker(Yu *et al.*, 2015) R package. We allowed a more strictly defined range of within 10kb upstream or 5kb downstream of the most proximal gene to determine binding status of that gene when producing results comparing association of peak and expression features with Treg and Tconv signatures.

Differential detection—To identify enriched sequences associated with p65 binding peaks, we used the SeqGL(Setty and Leslie, 2015) R package, which identifies nucleotide k-mers that discriminate positive peak sequences from negative sequences using logistic regression with sparse group lasso applied to related k-mer groups. We used both the default negative sequences of regions flanking peak summits (+/−150bp) but also provided custom sequences when appropriate. Additionally, SeqGL associates enriched k-mer groups to known binding motifs with the HOMER motif finding algorithm(Heinz *et al.*, 2010) (http://homer.ucsd.edu/homer/index.html). We report the SeqGL output which includes computed score for groups of k-mers along with the most similar known motif.

RNA-seq analysis—The reads were aligned with STAR v2.4.0c (Dobin *et al.*, 2013), and genes annotated in Gencode v18 were quantified with featureCounts v1.4.3-p1(Liao *et al.*, 2014). Normalization and differential expression was done with the Bioconductor package DESeq2(Love *et al.*, 2013).

Transposase-assessible chromatin (ATAC)-seq analysis—Publicly available ATAC-seq raw data for Treg and Tconv were obtained from a previous study (Kitagawa et al., 2017). Sequencing alignment was performed using Bowtie2 (Langead et al., 2012), and further analyzed by samtools in a general pipeline. ATAC-seq peaks were detected using HOMER. Annotation of normalized ATAC-seq peaks to ChIP-seq peaks in Treg and Tconv cells were performed using the annotatePeaks.pl program in HOMER package.

QUNATIFICATION AND STATISTICAL ANALYSIS

We used the unpaired Student t-test for two comparison groups. N represents the number of animals. Detailed description of statistics for each figure can be found in the figure legend. 5-way ANOVA was used to analyze the replicates of RNAseq.

To compare DNase I hypersensitivity signals in Treg and Tconv, we calculated the mean, quantile normalized, library-size normalized coverage signals using the ENCSR000COC and ENCSR000COA, respectively, from data made available by the mouse ENCODE Project. We calculated Mann-Whitney U test p-values comparing the Treg to Tconv signal over +/−150bp around peak summits for each peak set. We evaluated statistically associated features within the context of the previously described 587 Treg and 211 Tconv signature genes. One-sided Fisher exact tests were performed comparing the count of genes with affirmative binary status with regards to presence of an associated peak (within upstream 10kb to downstream 5kb), significant over-expression in Treg compared Tconv or WT compared to c-Rel/p65 DKO, or a member of the Treg signature instead of the Tconv signature.

KEY RESOURCES TABLE

REAGENT or RESOURCE	SOURCE	IDENTIFIER
Antibodies		
Anti-mouse CD4, APC-eFluor 780 conjugated, clone RM4-5	eBioscience	Catalog #47-0042-82
Anti-mouse CD8a, PE-CF594 conjugated, clone 53.6.7	BD Biosciences	Catalog #562315
Anti-mouse CD44, APC conjugated, clone IM7	Tonbo Biosciences	Catalog #20-0441
Anti-mouse CD62L, PE conjugated, clone MEL14	eBioscience	Catalog #12-0621-81
Anti-mouse CD25, APC conjugated, clone PC61.5	Tonbo Biosciences	Catalog #20-0251
Anti-mouse GITR, PE-Cy7 conjugated, clone DTA-1	eBioscience	Catalog #25-5874-80
Anti-mouse IFNγ PE conjugated, clone XMG1.2	BD Biosciences	Catalog #554412
Anti-mouse IL-17A APC conjugated, clone 17B17	eBioscience	Catalog #17-7177-81
Anti-mouse FoxP3 eFluor 450 conjugated, clone FJK16S	eBioscience	Catalog #48-5773-82
Polyclonal anti-p65, unconjugated, clone C-20	Santa Cruz	p65 C-20
Polyclonal anti-C-Rel, unconjugated, clone sc71	Santa Cruz	c-Rel SC-71
Monoclonal anti-mouse GAPDH, unconjugated, clone 6C5	Fitzgerald	Catalog #10R-G109a
In vivo mAb anti-mouse CD3, clone 145-2C11	BioXCell	Catalog #BE0001-1
Anti-mouse CD28, Na/Le	BioLegend	Catalog #102102
Bacterial and Virus Strains		
Biological Samples		
Chemicals, Peptides, and Recombinant Proteins		
IL-2, murine	Peprotech	Catalog #212-12
TGF-β1, human	Peprotech	Catalog #100-21C
Tat-cre	Protein and Proteomics Core Facility, The Children's Hospital of Philadelphia	N/A
ADCF-Mab media	HyClone/GE	Catalog #SH30349.01
Formaldehyde solution	Sigma	Catalog #F8775
Dynabeads Protein A	Invitrogen	Catalog #10002D

REAGENT or RESOURCE	SOURCE	IDENTIFIER
PMA salt	Sigma	Catalog #P8139
Golgi Plug protein transport inhibitor	BD Biosciences	Catalog #555029
Superscript IV reverse transcriptase	Invitrogen	Catalog #18090050
Veriquet Fast SYBR Fluor	Affymetrix	Catalog #75675
Ionomycin salt	Sigma	Catalog #10634
Collagenase type IV form C.Histolyticum	Sigma	Catalog #C5138
DNAse I from bovine pancreas	Sigma	Catalog #DN25
Critical Commercial Assays		
Magnisort mouse CD4 T cells enrichment kit	eBioscience	Catalog #8804-6821
Qiagen RNeasy Mini Kit	Qiagen	Catalog #74106
Qiagen RNeasy Micro Kit	Qiagen	Catalog #74004
CD4+ T cell isolation kit, mouse	Miltenyi	Catalog #130-104-454
Deposited Data		
RNAseq	GEO	GSE82076
ChIPseq	GEO	GSE99319
Experimental Models: Cell Lines		
Experimental Models: Organisms/Strains		
Mouse: *Rel*-Flox (Ulf Klein)	Heise et al., 2014	N/A
Mouse: *Rela*-Flox (Roland Schmid)	Algul et al., 2007	N/A
Mouse: *Foxp3*$^{tm4(YFP/icre)Ayr}$/J	Jackson laboratory	Stock #016959
Mouse: *Foxp3*$^{tm9(EGFP/cre/ERT2)Ayr}$/J	Jackson laboratory	Stock #016961
Mouse: *Gt(ROSA)26Sor*$^{tm1(EYFP)Cos}$/J	Jackson laboratory	Stock #006148
Mouse: *Cd4*cre	Jackson laboratory	Stock #022071
Mouse: *Foxp3*RFP (*Foxp3*^{tm1Flv}/J)	Jackson laboratory	Stock #008374
Mouse: *Rag1*^{tm1Mom}/J	Jackson laboratory	Stock #002216
Oligonucleotides		
Primer: FoxP3 forward: CCCATCCCCAGGAGTCTTG	Eurofins Genomics	
Primer: FoxP3 reverse: ACCATGACTAGGGGCACTGTA	Eurofins Genomics	
Primer: Ikzf2 forward: GAGCCGTGAGGATGAGATCAG	Eurofins Genomics	
Primer: Ikzf2 reverse: CTCCCTCGCCTTGAAGGTC	Eurofins Genomics	
Primer: Ikzf4 forward: TCTGGACCACGTCATGTTCAC	Eurofins Genomics	

REAGENT or RESOURCE	SOURCE	IDENTIFIER
Primer: Ikzf4 reverse: ACGATGTGGGAAGAGAACTCATA	Eurofins Genomics	
Primer: Cd83 forward: CGCAGCTCTCCTATGCAGTG	Eurofins Genomics	
Primer: Cd83 reverse: GTGTTTTGGATCGTCAGGGAATA	Eurofins Genomics	
Primer: Eomes forward: GCGCATGTTTCCTTTCTTGAG	Eurofins Genomics	
Primer: Eomes reverse: GGTCGGCCAGAACCACTTC	Eurofins Genomics	
Primer: Il13 forward: CCTGGCTCTTGCTTGCCTT	Eurofins Genomics	
Primer: Il13 reverse: GGTCTTGTGTGATGTTGCTCA	Eurofins Genomics	
Recombinant DNA		
Software and Algorithms		
Prism	GraphPad software	graphpad.com
FlowJo	FlowJo LLC	flowjo.com
Trim Galore! v0.4.1		https://www.bioinformatics.babraham.ac.uk/projects/trim_galore/
BWA mem	H. Li and Durbin, 2009	http://bio-bwa.sourceforge.net/
Picard suite of tools		http://broadinstitute.github.io/picard/
samtools	H. Li et al., 2009	http://samtools.sourceforge.net/
deepTools v2.3.6	Ramírez et al., 2016	http://deeptools.readthedocs.io/en/latest/#
phantompeakqualtools		https://www.encodeproject.org/software/phantompeakqualtools/
R		https://www.r-project.org/
WashU EpiGnome Browser	Zhou et al., 2011	http://epigenomegateway.wustl.edu/
MACS v2.1.1.20160309	Yong Zhang et al., 2008	https://github.com/taoliu/MACS
Irreproducible Discovery Rate (IDR) framework	Q. Li et al., 2011; Landt et al., 2012	https://sites.google.com/site/anshulkundaje/projects/idr
bedtools suite v2.25.0-24-g3d31735-dirty	Quinlan and Hall, 2010	http://bedtools.readthedocs.io/en/latest/
PePr algorithm	Yanxiao Zhang et al., 2014	https://github.com/shawnzhangyx/PePr
ChIPseeker	Yu et al., 2015	
SeqGL	Setty and Leslie, 2015	
HOMER motif finding algorithm	Heinz et al., 2010	http://homer.ucsd.edu/homer/index.html
STAR v2.4.0c	Dobin et al., 2013	
featureCounts v1.4.3-p1	Liao et al., 2014	
Bioconductor package DESeq2	Love et al., 2013	

REAGENT or RESOURCE	SOURCE	IDENTIFIER
Other		

Supplementary Material

Refer to Web version on PubMed Central for supplementary material.

Acknowledgments

References

Aschermann S, Lehmann CH, Mihai S, Schett G, Dudziak D, Nimmerjahn F. B cells are critical for autoimmune pathology in Scurfy mice. Proceedings of the National Academy of Sciences of the United States of America. 2013; 110:19042–19047. [PubMed: 24194550]

Algul H, Treiber M, Lesina M, Nakhai H, Saur D, Geisler F, Pfeifer A, Paxin S, Schmid RM. Pancreas-specific RelA/p65 truncation increases susceptability of acini to inflammtion-associated cell death following cerulein pancreatitis. J Clin Invest. 2007; 117:1490–501. [PubMed: 17525802]

Deenick EK, Elford AR, Pellegrini M, Hall H, Mak TW, Ohashi PS. c-Rel but not NF-kappaB1 is important for T regulatory cell development. Eur J Immunol. 2010; 40:677–681. [PubMed: 20082358]

Dobin A, Davis CA, Schlesinger F, Drenkow J, Zaleski C, Jha S, Batut P, Chaisson M, Gineras TR. STAR: ulatrafast universal RNA-seq aligner. Bioinformatics. 2013; 29:15–21. [PubMed: 23104886]

Gavin MA, Rasmussen JP, Fontenot JD, Vasta V, Manganiello VC, Beavo JA, Rudensky AY. Foxp3-dependent programme of regulatory T-cell differentiation. Nature. 2007; 445:771–775. [PubMed: 17220874]

Grigoriadis G, Vasanthakumar A, Banerjee A, Grumont R, Overall S, Gleeson P, Shannon F, Gerondakis S. c-Rel controls multiple discrete steps in the thymic development of Foxp3+ CD4 regulatory T cells. PloS one. 2011; 6:e26851. [PubMed: 22066012]

Heinz S, Benner C, Spann N, Bertolino E, Lin YC, Laslo P, Cheng JX, Murre C, Singh H, Glass CK. simple combination of lineage-determining transcription factors prime cis-regulatory elements required for machrophage and B ell identities. Mol Cell. 2010; 38:576–89. [PubMed: 20513432]

Heise N, De Silva NS, Silva K, Carette A, Simonetti G, Pasparakis M, Klein U. Germinal center B cell maintenance and differentiation are controlled by distinct NF-kB transcription factor subunits. J Exp Med. 2014; 211:2103–18. [PubMed: 25180063]

Isomura I, Palmer S, Grumont RJ, Bunting K, Hoyne G, Wilkinson N, Banerjee A, Proietto A, Gugasyan R, Wu L, et al. c-Rel is required for the development of thymic Foxp3+ CD4 regulatory T cells. J Exp Med. 2009; 206:3001–3014. [PubMed: 19995950]

Jana S, Jailwala P, Haribhai D, Waukau J, Glisic S, Grossman W, Mishra M, Wen R, Wang D, Williams CB, et al. The role of NF-kappaB and Smad3 in TGF-beta-mediated Foxp3 expression. Eur J Immunol. 2009; 39:2571–2583. [PubMed: 19701891]

Joshi SK, Hashimoto K, Koni PA. Induced DNA recombination by Cre recombinase protein transduction. Genesis. 2002; 33:48–54. [PubMed: 12001069]

Kerdiles YM, Stone EL, Beisner DR, McGargill MA, Ch' en IL, Stockmann C, Katayama CD, Hedrick SM. Foxo transcription factors control regulatory T cell development and function. Immunity. 2010; 33:890–904. [PubMed: 21167754]

Kitagawa Y, Ohkura N, Kidani Y, Vandenbon A, Hirota K, Kawakami R, Yasuda K, Motooka D, Nakamura S, Kondo M, et al. Guidance of regulatory T cell development by Satb1-dependent super-enhancer establishment. Nature immunology. 2017; 18:173–183. [PubMed: 27992401]

Landt SG, Mrinov GK, Kundaje A, Kheradpour P, Pauli F, Batzoglou S, Bernstein BE, Bickle P, Brown jb, Cayting p, Chen y, DeSalvo G, Epstein C, Fisher-Aylor KI, et al. ChIP-seq guidelines and practices of the ENCODE and modENCODE consortia. Genome Res. 2012; 22:1813–31. [PubMed: 22955991]

Langmead B, Salzberg SL. Fast gapped-read alignment with Bowtie 2. Nat Methods. 2012; 9:357–9. [PubMed: 22388286]

Levine AG, Arvey A, Jin W, Rudensky AY. Continuous requirement for the TCR in regulatory T cell function. Nature immunology. 2014; 15:1070–1078. [PubMed: 25263123]

Li H, Durbin R. Fast and accurate short read alignment with Burrows-Wheeler transform. Bioinformatics. 2009; 25:1754–60. [PubMed: 19451168]

Li H, Handsaker B, Wysoker A, Fennell T, Ruan J, Homer N, Marth G, Abecasis G, Durbin R. 1000 Genome Project Data Processing Subgroup. The Sequence Alignment/Map format and SAMtools. Bioinformatics. 2009; 25:2078–9. [PubMed: 19505943]

Li Q. Measuring reproducibility of high-throughput experiments. The Annals of Applied Statistics. 2011; 5:1752–1779.

Liao Y, Smyth GK, Shi W. featureCounts: an efficient general purpose program for assigninng sequence reads to genomic features. Bioinformatics. 2014; 30:923–30. [PubMed: 24227677]

Lio CW, Hsieh CS. A two-step process for thymic regulatory T cell development. Immunity. 2008; 28:100–111. [PubMed: 18199417]

Long M, Park SG, Strickland I, Hayden MS, Ghosh S. Nuclear factor-kappaB modulates regulatory T cell development by directly regulating expression of Foxp3 transcription factor. Immunity. 2009; 31:921–931. [PubMed: 20064449]

Love MI, Anders S, Kim V, Huber W. Differential analysis of RNA-seq data at the gene level using the DESeq2 package. 2013

Martin M. Cutadapt removes adaptor sequences from High-throughput sequencing reads. EMBnet Journal. 2011; 17(1)

Messina N, Fulford T, O' Reilly L, Loh WX, Motyer JM, Ellis D, McLean C, Naeem H, Lin A, Gugasyan R, et al. The NF-kappaB transcription factor RelA is required for the tolerogenic function of Foxp3(+) regulatory T cells. J Autoimmun. 2016; 70:52–62. [PubMed: 27068879]

Molinero LL, Yang J, Gajewski T, Abraham C, Farrar MA, Alegre ML. CARMA1 controls an early checkpoint in the thymic development of FoxP3+ regulatory T cells. J Immunol. 2009; 182:6736–6743. [PubMed: 19454668]

Ouyang W, Liao W, Luo CT, Yin N, Huse M, Kim MV, Peng M, Chan P, Ma Q, Mo Y, et al. Novel Foxo1-dependent transcriptional programs control T(reg) cell function. Nature. 2012; 491:554–559. [PubMed: 23135404]

Quinian AR, Hall IM. BEDTools: aflexible suite of utilities for comparing genomic features. Bioinformatics. 2010; 26:841–2. [PubMed: 20110278]

Ramirez F, Ryan DP, Gruning B, Bhardwaj V, Kilpert F, Richter AS, Heyne S, Dundar F, Manke T. deepTools2: anext generation web server for deep-sequencing data analysis. Nucleic Acid Res. 2016; 44:W160–5. [PubMed: 27079975]

Ruan Q, Kameswaran V, Tone Y, Li L, Liou HC, Greene MI, Tone M, Chen YH. Development of Foxp3(+) regulatory t cells is driven by the c-Rel enhanceosome. Immunity. 2009; 31:932–940. [PubMed: 20064450]

Rubtsov YP, Niec RE, Josefowicz S, Li L, Darce J, Mathis D, Benoist C, Rudensky AY. Stability of the regulatory T cell lineage in vivo. Science. 2010; 329:1667–1671. [PubMed: 20929851]

Samstein RM, Arvey A, Josefowicz SZ, Peng X, Reynolds A, Sandstrom R, Neph S, Sabo P, Kim JM, Liao W, et al. Foxp3 exploits a pre-existent enhancer landscape for regulatory T cell lineage specification. Cell. 2012; 151:153–166. [PubMed: 23021222]

Schuster M, Glauben R, Plaza-Sirvent C, Schreiber L, Annemann M, Floess S, Kuhl AA, Clayton LK, Sparwasser T, Schulze-Osthoff K, et al. IkappaB(NS) protein mediates regulatory T cell

development via induction of the Foxp3 transcription factor. Immunity. 2012; 37:998–1008. [PubMed: 23200824]

Setty M, Leslie CS. SeqGL Identifies Context-Dependent Binding Signals in Genome-Wide Regulatory Element Maps. PLoS computational biology. 2015; 11:e1004271. [PubMed: 26016777]

Soligo M, Camperio C, Caristi S, Scotta C, Del Porto P, Costanzo A, Mantel PY, Schmidt-Weber CB, Piccolella E. CD28 costimulation regulates FOXP3 in a RelA/NF-kappaB-dependent mechanism. Eur J Immunol. 2011; 41:503–513. [PubMed: 21268019]

Tone Y, Kidani Y, Ogawa C, Yamamoto K, Tsuda M, Peter C, Waldmann H, Tone M. Gene expression in the Gitr locus is regulated by NF-kappaB and Foxp3 through an enhancer. J Immunol. 2014; 192:3915–3924. [PubMed: 24634496]

Visekruna A, Huber M, Hellhund A, Bothur E, Reinhard K, Bollig N, Schmidt N, Joeris T, Lohoff M, Steinhoff U. c-Rel is crucial for the induction of Foxp3(+) regulatory CD4(+) T cells but not T(H)17 cells. Eur J Immunol. 40:671–676.

Wakamatsu E, Mathis D, Benoist C. Convergent and divergent effects of costimulatory molecules in conventional and regulatory CD4+ T cells. Proceedings of the National Academy of Sciences of the United States of America. 2013; 110:1023–1028. [PubMed: 23277554]

Ye CJ, Feng T, Kwon HK, Raj T, Wilson MT, Asinovski N, McCabe C, Lee MH, Frohlich I, Paik HI, et al. Intersection of population variation and autoimmunity genetics in human T cell activation. Science. 2014; 345:1254665. [PubMed: 25214635]

Yu G, Wang LG, He QY. ChIPseeker: an R/Bioconductor package for ChIP peak annotation, comparison and visualization. Bioinformatics. 2015; 31:2382–3. [PubMed: 25765347]

Zhang Y, Lin YH, Johnson TD, Rozek LS, Sator MA. PePr: a peak-calling prioritization pipeline to identify consistent or differential peaks from replicated ChIP-Seq data. Bioinformatics. 2014; 30:2568–75. [PubMed: 24894502]

Zhang Y, Liu T, Meyer CA, Eeckhoute J, Johnson DS, Bernsterin BE, Nusbaum C, Myers RMA, Brown M, Li W, Liu XS. Model-based analysis of ChIP-Seq (MACS). Gemone Biol. 2008; 9:R137.

Zhou X, Maricque B, Xie M, Li D, Sundaram V, Martin EA, Koebbe BC, Nielsen C, Hirst M, Farmham P, et al. The human epigenome browser at Washington University. Nat Methods. 2011; 8:989–90. [PubMed: 22127213]
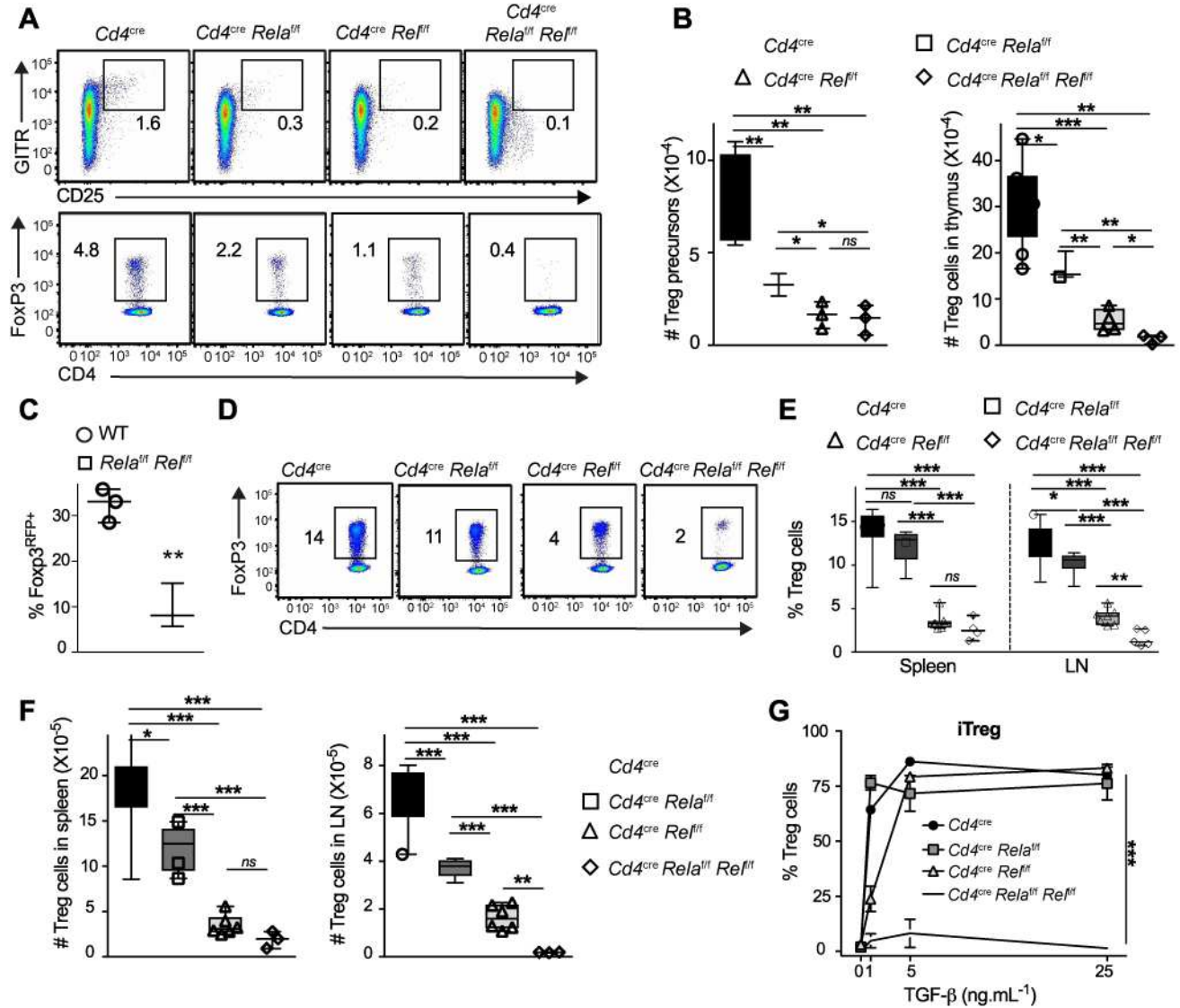
Figure 1. Discrete NF-κB subunits control sequential steps of Treg cell development

(A–B) Thymii from 5–7 weeks-old *Cd4*[cre] mice crossed to mice bearing floxed alleles of *Rela* and *Rel*, were analyzed by flow cytometry. (A) Representative dot plots of gated live CD4+CD8−FoxP3− (top) and CD4+CD8− cells (bottom). Numbers indicate the % of cells in each gate. (B) Absolute numbers of CD4+CD8−FoxP3−CD25+GITR+ Treg precursors (left) and CD4+CD8−FoxP3+ Treg cells. (C) CD4+CD8−FoxP3[RFP]−CD25+GITR+ cells were FACS-sorted from *Foxp3*[RFP] (WT) and *Foxp3*[RFP]*Rela*[f/f] *Rel*[f/f] thymii, treated with TAT-CRE and cultured with IL-2 for 2 days before analysis. Graph shows the % of FoxP3+CD25+ Treg in gated live cells. (D–F) FACS analysis of lymphoid tissues of mice described in (A). (D) Representative FoxP3 expression in gated live TCRβ+CD4+CD8−. Numbers indicate the percentage in the gate. (E, F) Percentage (E) and absolute numbers of TCRβ+CD4+CD8− FoxP3+ Treg cells (F). (G) CD4+CD25−CD44^{low} naïve T cells were sorted from the LN of indicated mice and stimulated with grading doses of hTGFβ. Graph shows the % of FoxP3+ among CD4+ cells after 4 days. In B, C, E and F, data is represented

as mean +/− SEM of at least 3 experiments (n=4–10 mice/group). *p<0.05, **p<0.01, ***p<0.001, n.s. non-significant. *See also* Figure S1.
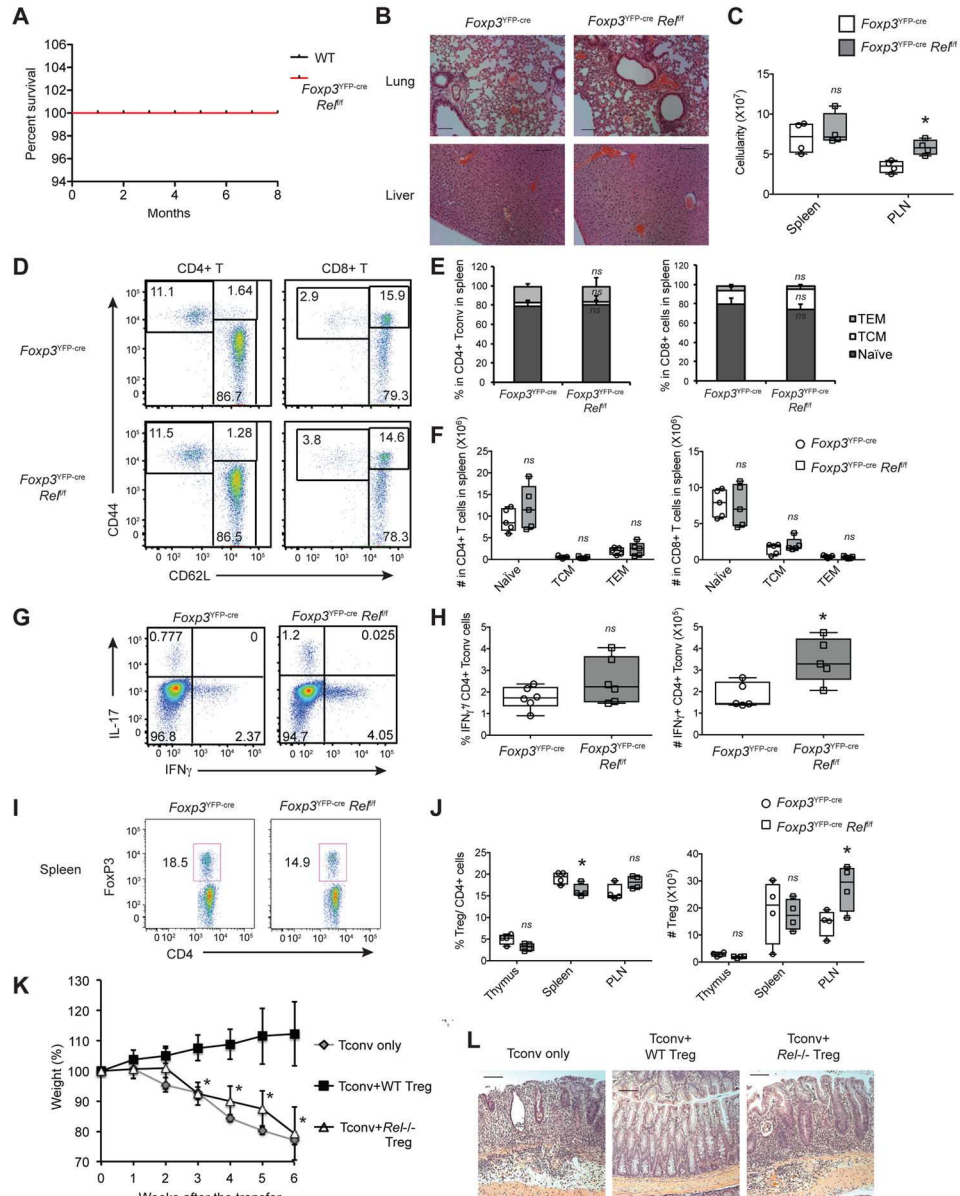
Figure 2. c-Rel is mainly dispensable for Treg homeostasis at steady-state
(A) Survival curves of WT (*Foxp3*[YFP-cre]*Rel*^{+/+}) and *Foxp3*[yfp-CRE]*Rel*[f/f] littermates. (B) H/E staining of lung and liver sections from 6-week old mice. Bars=100μm; original magnification: 100X. (C–J) Lymphoid tissues of 6-week old mice were analyzed by flow cytometry. (C) Total cell count in spleen and LN. (D) Representative CD44 and CD62L expression in spleen T cells. (E–F)% and numbers of naïve (CD44^{low}CD62L^{hi}), TCM (CD44^{hi}CD62L^{hi}) and TEM (CD44^{hi}CD62L^{low}) in spleen T cells. (G) Representative IL-17A and IFNγ expression in spleen CD4^{+} T cells. Numbers indicate the % in quadrants (H) % and numbers of IFNγ^{+}CD4^{+} T cells in spleen. (I) Representative FoxP3 expression in spleen CD4^{+} T cells. Numbers indicate the % in the gate. (J) Cumulative % and number of Treg cells in spleen. (K–L) *in vivo* colitis suppression assay. (K) Weight curves, shown as % of original weight. (L) Representative colon histology 6 weeks after transfer. Bars=100μm;

original magnification: 100X. In C and F–J, mean +/− SEM is shown. Data is representative or cumulative of 5 mice per group from two experiments. *p<0.05, **p<0.005. *See also* Figure S2.
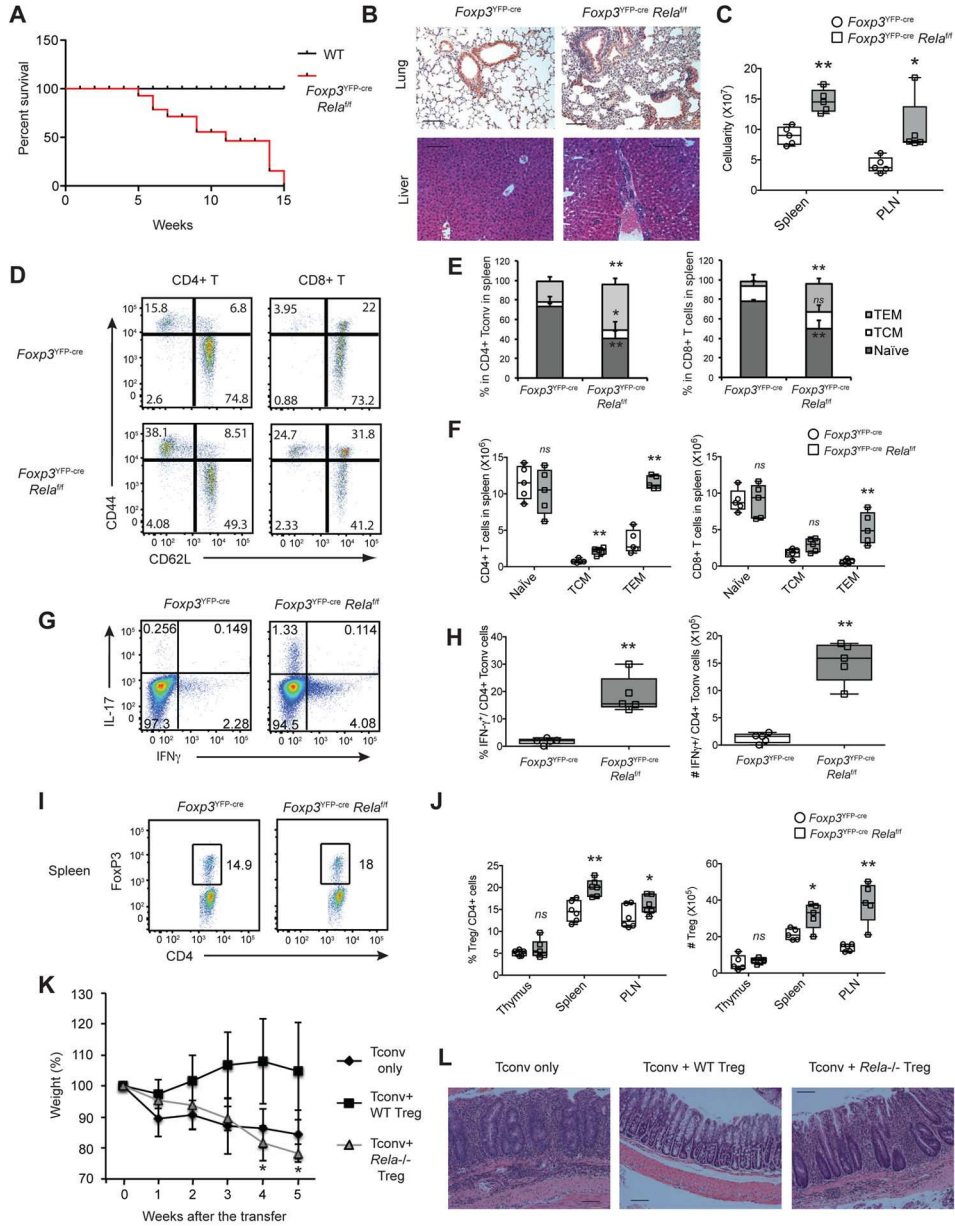
Figure 3. Mice lacking NF-κB p65 in Treg cells develop lethal autoimmune syndrome

(A) Survival curves of WT (*Foxp3*[YFP-cre]*Rela*^{+/+}) and *Foxp3*[YFP-cre]*Rela*[f/f] littermates. (B) H/E staining of lung and liver sections from 4–6 week-old mice. Bars=100μm; original magnification: 100X. (C–I) Lymphoid tissues of 4–6 week-old mice were analyzed by flow cytometry. (C) Total cell count in spleen and LN. (D) Representative CD44 and CD62L expression in spleen T cells. (E–F)% and numbers of naïve (CD44^{low}CD62L^{hi}), TCM (CD44^{hi}CD62L^{hi}) and TEM (CD44^{hi}CD62L^{low}) in spleen T cells. (G) Representative IL-17A and IFNγ expression in spleen CD4+ T cells. Numbers indicate the % in quadrants (H) % and numbers of IFNγ+CD4+ T cells in spleen. (I) Representative FoxP3 expression in spleen CD4+ T cells. Numbers indicate the % in the gate. (J) Cumulative % and number of Treg cells in spleen. (K–L) *in vivo* colitis suppression assay. (K) Weight curves, shown as %

of original weight. (L) Representative colon histology 5 weeks after transfer. Bars=100μm; original magnification: 100X. In C and F–J, mean +/− SEM is shown. Data is representative or cumulative of 5 mice per group from 3 experiments. *p<0.05, **p<0.005. *See also* Figure S3.
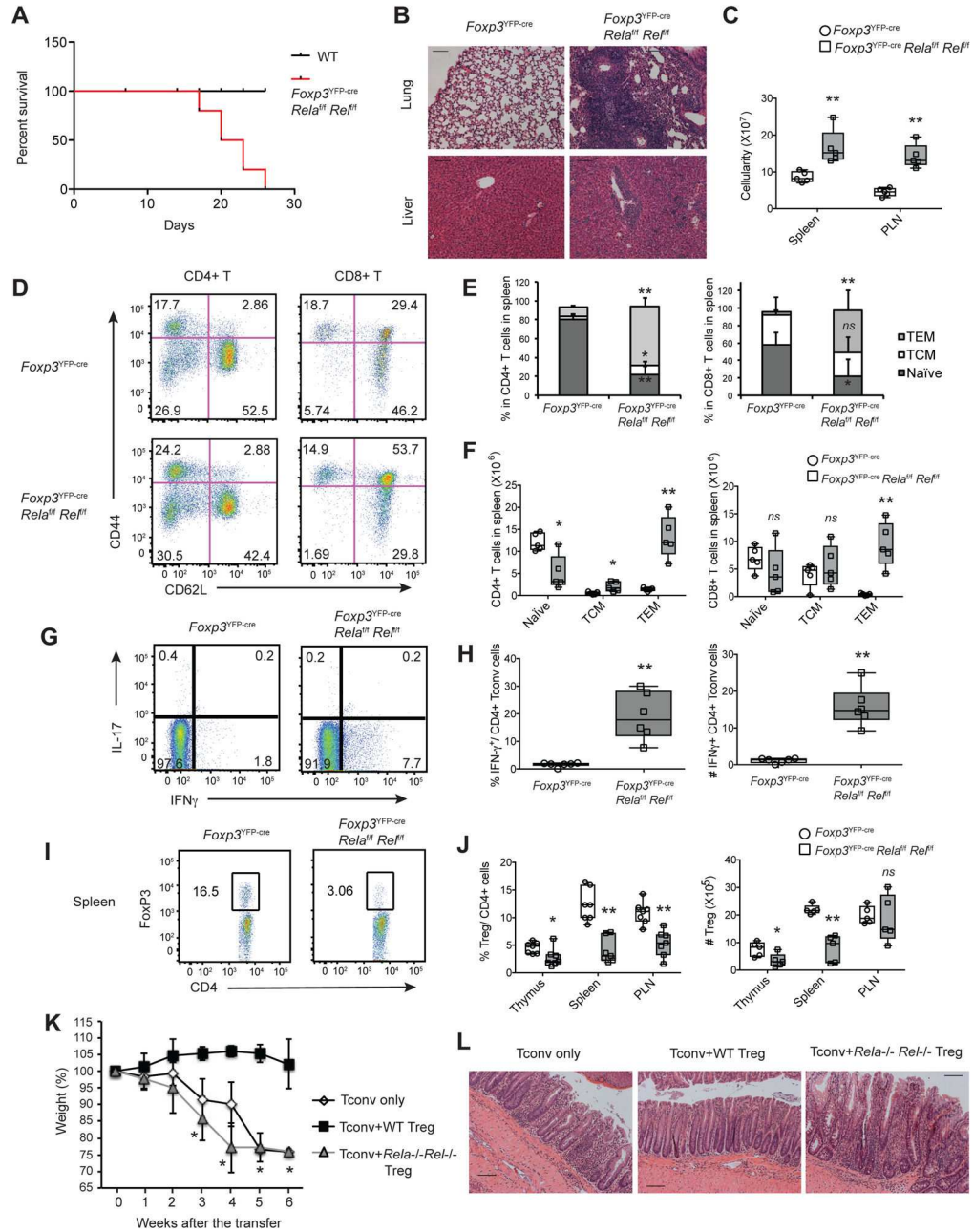
Figure 4. Complete ablation of the canonical NF-κB pathway drives a Scurfy-like autoimmune syndrome

(A) Survival curves of WT (*Foxp3*^YFP-cre^*Rela*^+/+^*Rel*^+/+^) and *Foxp3*^YFP-cre^*Rela*^f/f^*Rel*^f/f^ littermates. (B) H/E staining of lung and liver sections from 2–3-week old mice. Bars=100μm; original magnification: 100X. (C–I) Lymphoid tissues of 2–3 week-old mice were analyzed by flow cytometry. (C) Total cell count in spleen and LN. (D) Representative CD44 and CD62L expression in spleen T cells. (E–F)% and numbers of naïve (CD44^low^CD62L^hi^), TCM (CD44^hi^CD62L^hi^) and TEM (CD44^hi^CD62L^low^) in spleen T cells. (G) Representative IL-17A and IFNγ expression in spleen CD4+ T cells. Numbers indicate the % in quadrants. (H) % and numbers of IFNγ^+^CD4^+^ T cells in spleen. (I)

Representative FoxP3 expression in spleen CD4$^+$ T cells. Numbers indicate the % in the gate. (J) Cumulative % and number of Treg cells in spleen. (K–L) *in vivo* colitis suppression assay. (K) Weight curves, shown as % of original weight. (L) Representative colon histology 6 weeks after transfer. Bars=100μm; original magnification: 100X. In C and F–J, mean +/− SEM is shown. Data is representative or cumulative of 5 mice per group from two experiments. *p<0.05, **p<0.005. *See also* Figure S4.
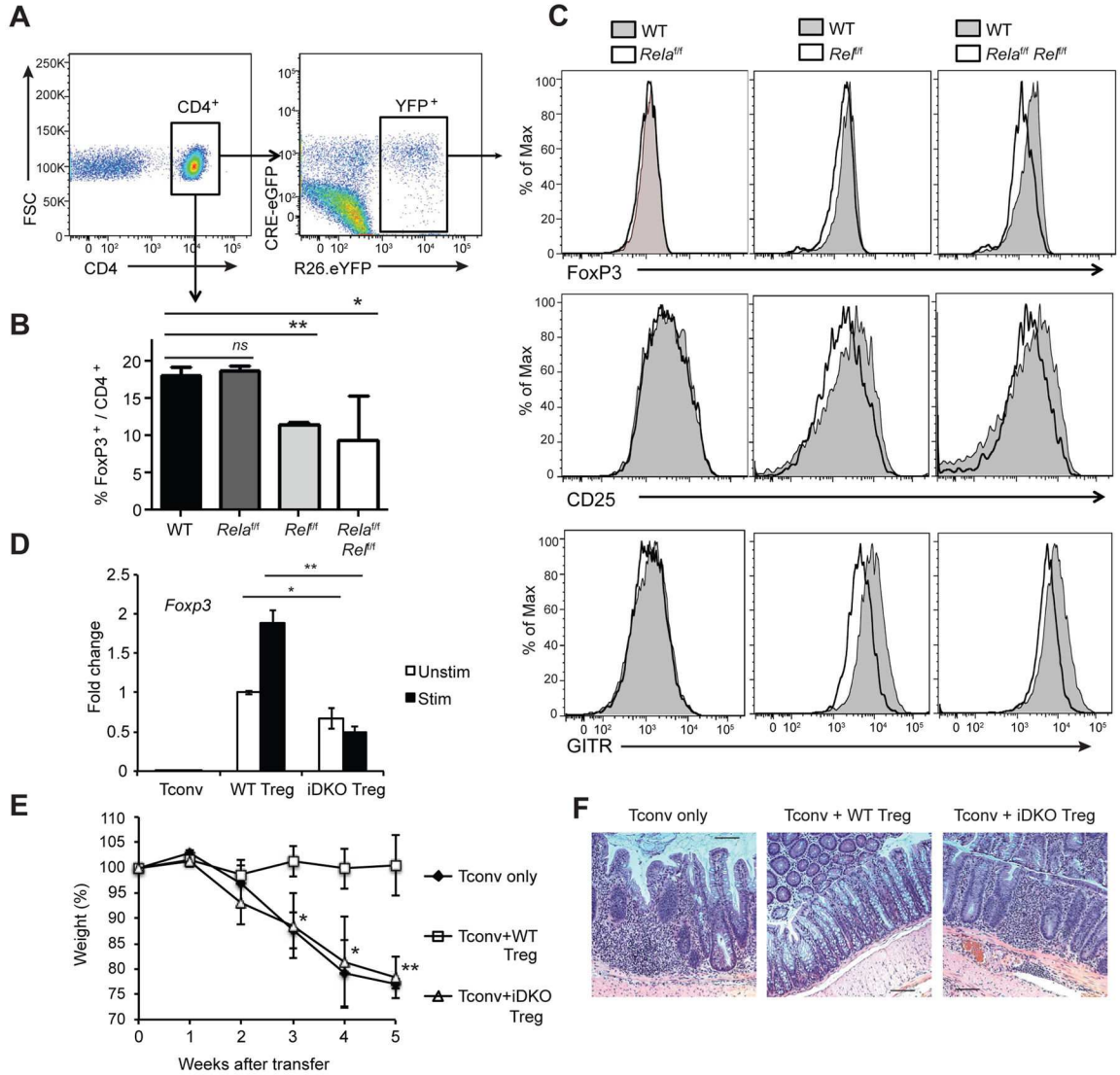
Figure 5. Tonic canonical NF-κB signaling maintains Treg homeostasis and function in peripheral mature Treg cells

(A) Inducible deletion of *Rela*, *Rel* or both *Rela* and *Rel* in Treg cells was achieved by tamoxifen treatment of *Foxp3*eGFP-Cre-ERT2x*Rosa26*stop-eYFP *Rela*f/f, *Rel*f/f and *Rela*f/f *Rel*f/f mice. YFP+ cells were gated from CD4+ cells and used for flow cytometry analysis. (B) Cumulative % of FoxP3+ Treg cells in total spleen CD4+ T cells. (C) YFP+ "recombined" Treg cells were sorted and stained for FoxP3, CD25 and GITR. A representative histogram is shown for each genotype. (D) Treg cells with inducible deletion of *Rela* and *Rel* after tamoxifen treatment were stimulated or not with anti-CD3 and anti-CD28 antibodies for 3 hours. RNA was prepared from those Treg cells and the expression level of *Foxp3* mRNA was examined by qPCR. The mean +/− S.D is shown. Data is representative of six mice per group from three experiments. (E–F) *in vivo* colitis suppression assay using sorted YFP+ recombined Treg cells. (E) Weight curves, shown as % of original weight. (F) Representative colon histology 5 weeks after transfer. Bars=100 μm; original magnification: 100X. In C and

F, mean +/− S.D is shown. Data is representative or cumulative of 5 mice per group from 3 experiments. *p<0.05, **p<0.005.
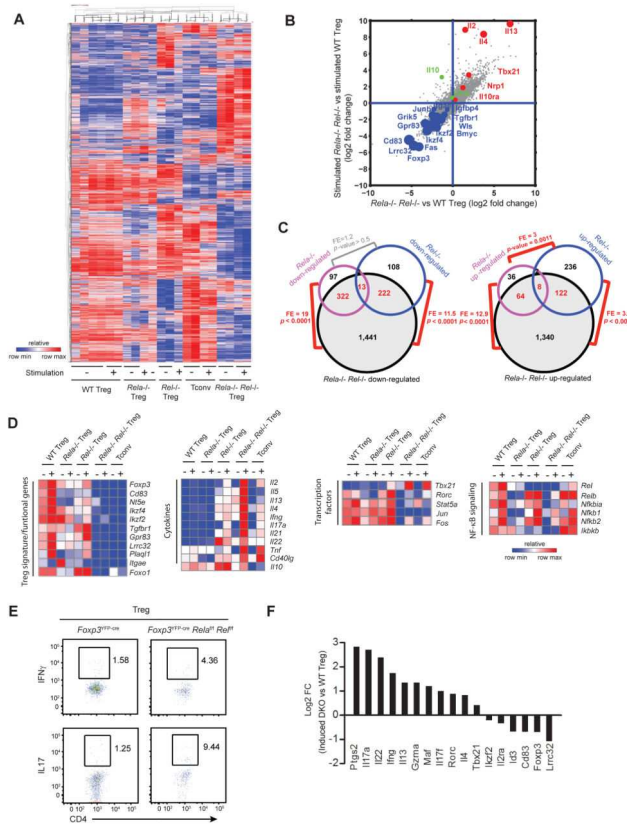
Figure 6. Canonical NF-κB shapes the molecular identity of Treg cells

Treg and Tconv cells of the indicated genotypes were FACS-sorted, *in vitro*-activated or not for 3 hours and submitted to RNAseq. (A) Heatmap created by unsupervised hierarchical gene clustering shows normalized expression of transcripts whose expression was changed in at least 1 condition (FC>1, ANOVA p<0.05). (B) Log^2 fold changes of $Rela^{-/-}Rel^{-/-}$ Treg versus WT Treg and stimulated $Rela^{-/-}Rel^{-/-}$ Treg versus stimulated WT Treg. Representative genes from down-regulated genes were indicated as blue and representative genes from upregulated genes were indicated as red. The size of the selected genes indicates p-values by ANOVA. (C) 5-way ANOVA analysis was performed to assess the association between genes and different factors (factor 1: Treg or Tconv; factor 2: stimulated or not; factor 3: $Rela^{-/-}Rel^{-/-}$ or not; factor 4: $Rela^{-/-}$ or not; factor 5: $Rel^{-/-}$ or not). The Venn diagrams depict downregulated (top) and upregulated (bottom). (D) Representative genes from the genes with significantly changed expression in $Rela^{-/-}Rel^{-/-}$ Treg cells were categorized by their function and the expression change was presented as heatmaps. (E) Representative flow cytometry plots from intracellular staining for IFNγ and IL-17 in CD4$^+$ FoxP3$^+$ Treg cells from *Foxp3*$^{YFP-cre}$ and *Foxp3*$^{YFP-cre}$ $Rela^{f/f}Rel^{f/f}$. (F) Treg cells were isolated from *Foxp3*$^{eGFP-Cre-ERT2}$x*Rosa26*$^{stope-YFP}$ WT and *Foxp3*$^{eGFP-Cre-ERT2}$x*Rosa26*$^{stop-eYFP}$ $Rela^{f/f}Rel^{f/f}$ after tamoxifen treatment and expression of various genes were examined by qPCR. Log^2 fold changes (Log$_2$ FC) of gene expression in inducible DKO versus WT were shown. *See also* Figure S5.
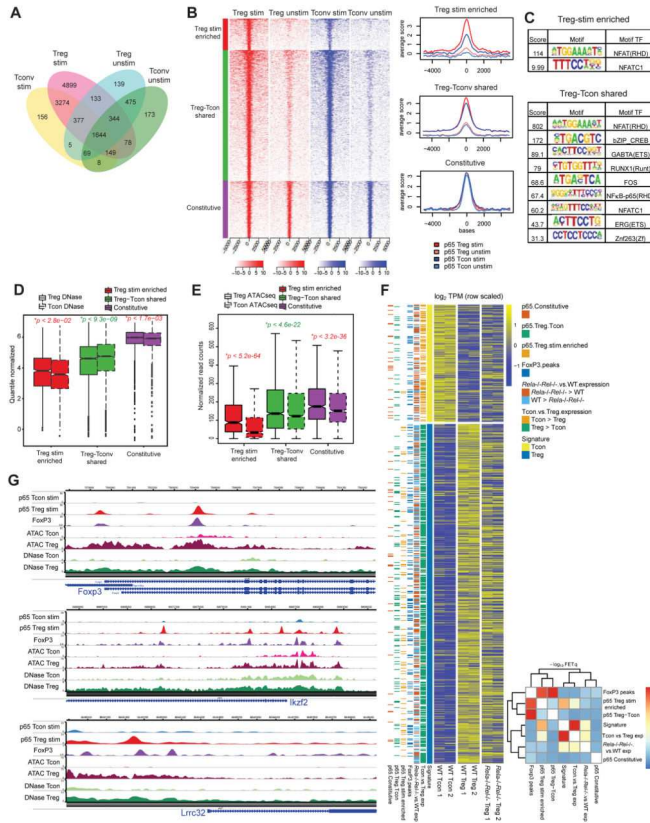
Figure 7. NF-κB regulates the Treg-associated transcriptional program

(A–F) WT Tconv and Treg cells were isolated and stimulated or not for 3 hours. p65 ChIP was performed and subjected to library preparation and sequencing as described in the Methods section. (A) The Venn diagram represents the number of p65-binding peaks and overlapping and non-overlapping peaks between four groups. (B) Heatmap showing the distribution of mean $\log_2$ p65-ChIP/input signal for Treg stim/unstim (red) and Tconv stim/unstim (blue) around peaks summits, +/− 5kb flanks from TSS, from each group: Treg-specific (red bar), Treg-Tconv shared (green bar) and constitutive (purple bar). The log2 p65-ChIP/input signal is also presented as histograms on the right. (C) Enrichment of motifs in Treg-specific peaks and Treg-Tconv shared peaks as determined by the SeqGL algorithm. (D) Comparison of quantile normalized, library-size normalized, DNase accessibility signals between Treg and Tconv around summits (+/−150bp) of three different peak sets. Mann-Whitney U test *P* values comparing Treg vs. Tcon signal are also provided. (E) Comparison of ATAC-seq signals between Treg and Tconv of three different peak sets. (F) The log2 TPM counts for two sets of RNAseq data for Tconv, WT Treg and $Rela^{-/-}Rel^{-/-}$ Treg (Right side columns of the heatmap) corresponding to Tconv signature and Treg signature genes were displayed as a heatmap. Genes with significant expression changes in $Rela^{-/-}Rel^{-/-}$ vs WT Treg and Tconv vs Treg were indicated. Genes, within its −10kb to +5kb coordinates, associated with p65 constitutive peaks, Tconv-Treg shared peaks, Treg stim-specific peaks and FoxP3 peaks are also indicated along the leftside of the heatmap. The cluster heatmap shows the pairwise −log10 p-values for fisher exacts comparing the indicated annotation groups. (G) Example genes from the set of genes including p65 Treg stim-enriched peaks.

Tracks were created in WashU epigenome browser and display normalized p65, FoxP3, ATAC-seq and DNase HS sequencing signal. *See also* Figure S6.